Dlx1/2-Dependent Expression of *Meis2* Promotes Neuronal Fate Determination in the Mammalian Striatum

Zihao Su[1,3], Ziwu Wang[1,3], Susan Lindtner[2], Lin Yang[1], Zicong Shang[1], Yu Tian[1], Rongliang Guo[1], Yan You[1], Wenhao Zhou[1], John L. Rubenstein[2], Zhengang Yang[1] and Zhuangzhi Zhang[1,‡]

[1]Key Laboratory of Birth Defects, Children's Hospital of Fudan University, State Key Laboratory of Medical Neurobiology and MOE Frontiers Center for Brain Science, Institutes of Brain Science, Fudan University, 138 Yi Xue Yuan Road, Shanghai 200032, China.

[2]Department of Psychiatry, Nina Ireland Laboratory of Developmental Neurobiology, UCSF Weill Institute for Neurosciences, University of California, San Francisco, CA 94158, USA.

[3]These authors contributed equally to this work.

[‡]**Correspondence**

Zhuangzhi Zhang, Email: zz_zhang@fudan.edu.cn;

ABSTRACT

The striatum is a central regulator of behavior and motor function through the actions of D1 and D2 medium-sized spiny neurons (MSNs), which arise from a common lateral ganglionic eminence (LGE) progenitor. The molecular mechanisms of cell fate specification of these two neuronal subtypes are incompletely understood. Here, we found that deletion of *Meis2*, which is highly expressed in the LGE and derivatives led to a large reduction in striatal MSNs due to a block in their differentiation. *Meis2*

2022. Published by The Company of Biologists Ltd.

directly binds to the *Zfp503* and *Six3* promoters and is required for their expression and specification of D1 and D2 MSNs, respectively. Finally, *Meis2* expression is regulated by *Dlx1/2* at least partially through the enhancer *hs599* in the LGE SVZ. Overall, our findings define a pathway in the LGE whereby *Dlx1/2* drives expression of *Meis2* which subsequently promotes the fate determination of striatal D1 and D2 MSNs via *Zfp503* and *Six3*.

KEYWORDS: ***Meis2*, *Six3*, *Zfp503, Dlx1/2,* Striatum, LGE**

INTRODUCTION

The striatum is first component of the basal ganglia that receives cortical input; it participates in computations that mediate complex movements, reward learning, decision making, emotion and cognition (Hikida et al., 2010; Hintiryan et al., 2016; Valjent and Gangarossa, 2020; Xiao et al., 2020). In mammals, the majority of striatal neurons are GABAergic medium-sized spiny neurons (MSNs), which can be subdivided into two subpopulations according to their transcriptional profile and target innervation (Doyle et al., 2008; Gerfen and Surmeier, 2011; Lobo et al., 2006). Striatonigral neurons (D1 MSNs) are characterized by the transcription factors (TFs) *Zfp503* and *Isl1* and specifically express the dopamine D1 receptor (DRD1) and the neuropeptide TAC1 (known as substance P) (Chen et al., 2020; Ehrman et al., 2013; Gerfen et al., 1990; Gerfen and Surmeier, 2011; Lu et al., 2014; Soleilhavoup et al., 2020). In contrast, striatopallidal neurons (D2 MSNs) are characterized by the *Sp8/9* and *Six3* TFs, and specifically express the dopamine D2 receptor (DRD2) and the neuropeptide enkephalin (ENK) (Gerfen et al., 1990; Gerfen and Surmeier, 2011; Gokce et al., 2016; Lobo et al., 2006; Stanley et al., 2019; Xu et al., 2018; Zhang et al., 2016). Both cell types originate from a common pool of progenitor cells located in the lateral ganglionic eminence (LGE) and express TFs such as *Gsx1/2*, *Ascl1* and *Dlx1/2* (Anderson et al., 1997; Bocchi et al., 2021; Kelly et al., 2018; Long et al., 2009b; Pei et al., 2011; Wang et al., 2013; Yun et al., 2002). The molecular mechanisms of that specify D1 and D2 MSNs remain to be fully elucidated.

Homeodomain TFs comprise a large family of evolutionarily conserved DNA binding proteins that have a myriad of roles in controlling animal development (Gehring et al., 1994).The *Meis1/2/3* homeodomain TFs belong to the three amino acid loop extension (TALE) family of homeodomain proteins, that include the PBX and PKNOX families; together they play important roles in development and disease in part through modulating the function of HOX TFs (Golonzhka et al., 2015; Moens and Selleri, 2006; Mukherjee and Burglin, 2007). In nonneuronal tissues, *Meis2* regulates the proliferation, differentiation and survival in the limbs, craniofacial skeleton and heart (Cunningham and Duester, 2015; Machon et al., 2015; Wang et al., 2020; Zha et al., 2014). Furthermore, *Meis2* plays pivotal roles in the gene regulatory network driving the differentiation of human embryonic stem cells towards cardiovascular cell types (Paige et al., 2012). *Meis2* loss of function causes a triad of palatal defects, congenital heart defects, and intellectual disability in humans (Giliberti et al., 2020; Verheije et al., 2019). Although the expression of *Meis2* in the central nervous system was reported twenty years ago (Larsen et al., 2010; Toresson et al., 1999), its functions in the forebrain remain to be investigated. Furthermore, investigation of the molecular mechanisms by which *Meis2* regulates the development of MSNs may provide a theoretical and experimental basis for clinical applications to disorders of the basal ganglia.

The present study was undertaken to uncover the molecular mechanisms of *Meis2* in regulating the development of striatal MSNs. In the *Meis2*-conditional knockout (CKO) (*Dlx5/6-CIE; Meis2*$^{F/F}$) mouse, LGE precursor cells failed to fully differentiate into MSNs leading to an expansion of the subventricular zone (SVZ). As a result, the majority of MSNs were not generated. Analysis of the results of RNA sequencing (RNA-seq), Assay for Transposase-Accessible Chromatin using sequencing (ATAC-seq) and Cleavage Under Targets and Tagmentation with sequencing (CUT&Tag-seq) experiments revealed that *Six3* and *Zfp503* are critical direct downstream targets of *Meis2* in controlling the specification of the D1 and D2 MSNs. Furthermore, the results of single-cell ATAC-seq and chromatin immunoprecipitation

with sequencing (ChIP-seq) (Lindtner et al., 2019) showed that DLX1/2 directly bind to the three *Meis2* distal enhancer elements (*hs355*, *hs599* and a 3rd putative enhancer) to promote *Meis2* expression in the LGE. Finally, deletion of *hs599* led to a significant decrease in the expression of *Meis2* in the LGE SVZ. Taken together, our findings suggest that *Meis2* promotes the precursor specification in D1 and D2 MSNs by directly promoting the expression of *Six3* and *Zfp503*, respectively. Moreover, *Meis2* expression is dependent on *Dlx1/2* in the LGE SVZ, and this regulation is at least partially mediated by the *hs599* enhancer.

RESULTS

Meis2 is highly expressed in the lateral ganglionic eminence (LGE) and striatum

To study the distribution of *Meis2* in the ganglionic eminences, we performed a detailed analysis of *Meis2* mRNA by in situ hybridization (ISH). We observed a high level of *Meis2* in the LGE SVZ and a moderate level in the ventricular zone (VZ). In contrast, *Meis2* expression was nearly absent from the globus pallidus, a major nucleus generated by the medial ganglionic eminence (MGE) (Fig. 1A and Fig. S1A). At E16.5, P0 and in the adult, *Meis2* continues to be strongly expressed in the entire striatum (Figs. S1B-D). ASCL1/MEIS2/BCL11B triple immunofluorescence staining at E14.5 found that very few ASCL1-positive cells were co-labeled with MEIS2 in the LGE suggesting that MEIS2 is not strongly expressed in dividing cells of the SVZ (Figs. S1E-F). Most striatal medium-sized spiny neurons (MSNs) express BCL11B (Arlotta et al., 2008; Zhang et al., 2019). As nearly all BCL11B-positive LGE cells also express MEIS2, providing evidence that MEIS2 is expressed in striatal neurons (Figs. S1E-F). Finally, we found that all MEIS2-positive cells also expressed the striatal pan-neuronal marker FOXP1 at P30 (Figs. S1G-J). Altogether, our results showed that *Meis2* is principally expressed in MSNs from embryonic to adult stages.

Nearly all striatal MSNs are lost in *Meis2*-conditonal knockout (CKO) mice

To investigate the role of *Meis2* in the LGE (striatal primordium), we crossed a *Dlx5/6-CIE* mouse with a *Meis2*$^{F/+}$ line to eliminate *Meis2* expression in the SVZ and MZ of the LGE (Fig. 1B). We referred to the conditional mutant as *Meis2*-CKO. First, we identified differentially expressed (DE) genes between *Meis2*-CKO mice and control mice via RNA-seq analysis from the LGE at E14.5. We identified 161 genes with downregulated RNA expression and 95 genes with upregulated RNA expression (Table 1). Next, we performed gene ontology (GO) analysis on the 256 dysregulated genes. This analysis suggests that *Meis2* is mainly involved in the positive regulation of neuron differentiation, axonogenesis and forebrain development (Fig. 1C). Genes expressed in immature and/or mature MSNs, such as *Aldh1a3*, *Zfp503* and *Six3* were downregulated. In contrast, the genes expressed in proliferating cells, such as *Wnt5a*, *Pcna* and *Dlx1* were upregulated (Fig. 1D and Table 1). Finally, we selected 8 genes that are highly expressed in MSNs (*Foxp1*, *Rarb*, *Rxrg*, *Ikzf1*, *Ebf1*, *Foxp2*, *Penk* and *Bcl11a*) and examined expression in the *Meis2*-CKO via ISH or immunofluorescence (Fig. 1E; Figs. S2A-J). Our results showed that the expression of these genes was greatly reduced in the *Meis2*-CKO mice compared to the control mice. Overall, these findings showed that *Meis2* plays a central transcriptional role in the generation of striatal MSNs.

Accumulation of progenitors in the LGE SVZ of *Meis2*-CKO mice

Next, we explored the mechanism underlying the failure of the *Meis2*-CKO mutants to generate MSNs. First, we tested whether *Meis2* affects the proliferation of LGE progenitors, and thus examined the expression of markers of LGE cell proliferation: GSX2, ASCL1 and PCNA (Anderson et al., 1997; Castro et al., 2011; Chapman et al., 2013) at E16.5 (Figs. 2A-F). GSX2 and ASCL1 were expressed in the radial glia cells and intermediate progenitors in the LGE (Chapman et al., 2013; Wang et al., 2013; Zhang et al., 2020) and we found that the number of GSX2 and ASCL1 positive cells were increased in *Meis2*-CKO mutants (Figs. 2A-D and K). Analysis of the number of cycling cells at E16.5 in *Meis2*-CKO and control mice showed that the total number of

proliferating cells in the SVZ was increased, inducing an enlargement of the proliferative area stained with PCNA (Figs. 2E-F and K). This increase results in an enlarged SVZ and a very small striatum. The distal-less homeobox genes (*Dlx1/2* and *Dlx5/6*) are essential for the MSN differentiation in the LGE (Anderson et al., 1997; Fazel Darbandi et al., 2016; Lindtner et al., 2019; Long et al., 2009a; Wang et al., 2013; Wang et al., 2011; Yun et al., 2002). The *Dlx* genes are highly expressed in LGE progenitor cells (largely in the SVZ) (Liu et al., 1997; Zhang et al., 2016). Our results showed that the number of cells expressing DLX2, CRE (driven by a *Dlx5/6* enhancer), and *Dlx5* (mRNA) were increased in the *Meis2*-CKO LGE SVZ compared to control mice (Figs. 2G-K; Figs. S2K-L).

To further confirm that *Meis2* affects the proliferation of LGE precursors, we used another *Cre* line (*Gsx2-Cre*) to conditionally knock out *Meis2* in the VZ and SVZ of the LGE. Using KI67, BrdU incorporation (2 h) and PH3, confirmed that *Meis2* mutants accumulated progenitors in the LGE SVZ at E14.5 or E16.5 (Figs. S3A-D). Taken together, these results indicated that *Meis2* is required for LGE progenitors to leave the cell cycle, and as a result *Meis2* mutants accumulate proliferating cells in the LGE SVZ.

Abnormal accumulation of the immature MSNs in the LGE SVZ of *Meis2*-CKO mice

Previously we showed that the *Sp8* and *Sp9* TFs are required for the differentiation of the D2 MSNs in the ventral LGE (vLGE) (Xu et al., 2018; Zhang et al., 2016). These TFs are highly expressed in the LGE SVZ and striatum. Here we found that the SP8- and SP9-positive cells were increased in the *Meis2*-CKO LGE SVZ (Figs. 3A-D and K and Figs. S2O-P). Because *Sp8/9* are expressed in progenitors and postmitotic neurons (MSNs), we explored whether these cells were proliferating or postmitotic, we examined the expression of markers of immature neurons, TUBB3 and doublecortin (DCX). There were robust TUBB3 and DCX expressions in the expanded LGE SVZ of the *Meis2*-CKO (Figs. 3E-H and Fig. 3L). In addition, we found that many immature neurons which expressed *Gad1* were located in the LGE SVZ of

Meis2-CKO mice (Figs. 3I-J and Fig. 3L). Next, we want to further confirm these phenotypes at later stage. Because the *Meis2*-CKO mice only survive several hours after birth, we analyzed the *Meis2*-CKO mice at P0. *Meis2*-CKO P0 mice had an enlarged ventricle and a small striatum (Figs. 4A-B). In the rostral LGE the *Sp8* and *Bcl11b* TFs are mainly expressed in the SVZ (neuroblast) and MSNs, respectively (Arlotta et al., 2008; Li et al., 2017; Waclaw et al., 2006; Xu et al., 2018). We found some BCL11B-positive cells were generated, but they were significantly reduced in the *Meis2*-CKO striatum at P0 (Figs. 4A-B). We also found the SP8-positive cells were present in the enlarged SVZ (Figs. 4C-D). Combined with our previous study (Yang et al., 2021b), we speculated that the cells were gradually depleted in the LGE due to abnormal differentiation. Taken together, these results suggested that in the absence of *Meis2*, progenitor cells and immature neurons cannot differentiate well into striatal mature MSNs.

Meis2 is required for the differentiation of the olfactory bulb interneuron

The LGE consists of subdomains including the dorsal LGE (dLGE) and ventral LGE (vLGE) (Wen et al., 2021; Yun et al., 2001). The progenitors located in the dLGE contribute to the olfactory bulb (OB) interneurons, whereas vLGE progenitors mainly generate striatal MSNs (Li et al., 2017; Li et al., 2021; Song et al., 2021; Waclaw et al., 2006; Waclaw et al., 2009; Xu et al., 2018; Yang et al., 2021a; Zhang et al., 2016). In the *Meis2*-CKO at E16.5 the dLGE marker *Sp8* was expanded ventrally, but the expression of the *Etv1* (another dLGE marker) was not significantly altered (Figs. 3C-D and Figs. S2M-P). Therefore, these results indicated that the expansion of the SP8 positive cells in the LGE are likely to be the immature MSNs of abnormal differentiation. Next, we wonder whether the OB interneurons and striatal MSNs were affected in the *Meis2*-CKO mice.

Next, we studied SP8, CB, TH and PAX6 expression in the OB at P0 in the *Meis2*-CKO mice compared to control mice. We found that the expression of SP8 had increased in GCL (slight increase of CB as well), but decreased in the GL (Figs. 4E-H and M-N). Almost all TH-positive OB interneurons were lost in the GL in the

Meis2-CKO mice compared to their controls (Figs. 4I-J and M). Moreover, the expression of the *Pax6* which is required for the differentiation of the OB TH-positive interneurons was also significantly reduced in the GL in the *Meis2*-CKO mice compared to their controls (Figs. 4K-M), consistent with a previous study showing that *Meis2* is required for the differentiation of the TH-positive OB interneurons in the adult neurogenesis. Taken together, *Meis2* is required for the differentiation of OB periglomerular interneurons.

Meis2 controls MSN fate through promoting _Six3_ and _Zfp503_ expression

To gain insights into the mechanism of *Meis2* in regulating the differentiation of striatal MSNs, we focused on our RNA-seq. The TF genes *Six3*, *Zfp503*, *Isl1*, and the *Aldh1a3 gene,* caught our attention because their RNA expression was significantly reduced in *Meis2*-CKO mice. Furthermore, MEIS2 binds to the putative promoters (< 3 kb of the TSS) of *Six3, Zfp503, Aldh1a3 and Isl1* (Figs. 5A-B; Fig. S4A). As expected, the expression of these genes, detected by in situ hybridization or immunostaining, was significantly decreased in *Meis2*-CKO mice (Fig. 5D; Fig. S4B). Moreover, our results showed that the number of D2 MSNs (specifically expressing *Drd2* and *Adora2a*) and D1 MSNs (specifically expressing EBF1 and FOXP2) (Gokce et al., 2016; Lobo et al., 2006; Lobo et al., 2008; Stanley et al., 2019; van Rhijn et al., 2018; Zhang et al., 2016) were greatly decreased in *Dlx5/6-CIE; Six3*$^{F/F}$ (*Six3*-CKO) and *Dlx5/6-CIE; Zfp503*$^{F/F}$ (*Zfp503*-CKO) mice, respectively (Figs. S4C-D). In other words, the TFs *Six3* and *Zfp503* are crucial for the generation of D2 and D1 MSNs, respectively. These phenotypes are very similar to those of *Meis2*-CKO mice and are consistent with previous reports (Chen et al., 2020; Soleilhavoup et al., 2020; Song et al., 2021; Xu et al., 2018).

Finally, to test the ability of MEIS2 to regulate transcription of putative promoters of *Six3* and *Zfp503*, we performed a dual-luciferase transcription activation assay using the N2a cell line. MEIS2 robustly activated transcription from these promoters (Fig.

5C). Overall, our findings suggested that the TF *Meis2* promotes fate determination of striatal MSNs by directly promoting *Six3* and *Zfp503* expression.

***Dlx1/2* are required for the expression of *Meis2* in the LGE**

Meis2 is highly expressed in the LGE and its derivatives and is a key factor for the normal development of MSNs. Hence, we wondered which genes can promote the expression of *Meis2* in the striatum. A previous study showed that *Dlx1/2* were required for the normal development of the striatal SVZ and the differentiation of MSNs (Anderson et al., 1997). Furthermore, the phenotypes of the *Dlx1/2* mutant mice were very similar to those of *Meis2*-CKO mice; these mutant mice had an enlarged LGE SVZ (containing many proliferating cells and undifferentiated cells) and a very small striatum (lacking mature MSNs) (Anderson et al., 1997). Therefore, we analyzed *Dlx1/2* mutant mice and found that the expression of *Meis2* was greatly reduced in the LGE SVZ of the *Dlx1/2* mutant mice (Fig. 6A) (Long et al., 2009b). Next, to test whether *Dlx1/2* directly regulate *Meis2* expression, we analyzed the *Dlx1/2* ChIP-seq data of E11.5, E13.5 and E16.5 LGE (Lindtner et al., 2019). This gave us a chance to systematically analyze the downstream targets of *Dlx1/2* in the LGE. As expected, we observed three *Dlx1/2* binding regions near the *Meis2* gene body (Fig. 6B). Two of the three regions are named as *hs355* and *hs599*. Then, we performed a luciferase reporter assay in N2a cells. Cotransfection of cells with a DLX2 expression vector (pCS2-*Dlx2*) with the enhancer-reporter construct (pGL4.23-*Meis2-hs355*, R1 or *hs599*) resulted in an ~7-fold increase in pGL4.23-*Meis2-hs599* luciferase activity compared with that of the pGL4.23 empty luciferase control (Fig 6C). As in previous reports, *hs599* showed enhancer activity in the developing striatum (McGregor et al., 2019; Silberberg et al., 2016; Visel et al., 2013). Thus, we focused on the function of *hs599* in regulating *Meis2* expression. To examine the in vivo function of *hs599*, we used CRISPR/Cas9 genome editing in fertilized eggs to generate *hs599* heterozygous mice (Fig. 6D and Figs. S6E-H). We then analyzed the expression of *Meis2* in *hs599* mutant mice at E14.5 and E16.5. Our results showed that the expression of *Meis2* was reduced in the LGE SVZ (Figs. 6E-F). This provides

functional evidence that *hs599* is a *Meis2* enhancer in the LGE SVZ. Surprisingly, the development of the LGE seems normal in *hs599* mutant mice (Figs. S5A-F). We speculated that there needs to be a loss of a specific threshold of *Meis2* expression to yield a striatal phenotype and the *hs599* mutant mice have reduced *Meis2* expression but are not at the level necessary for the striatal phenotype. Taken together, our findings suggested that *Dlx1/2* promote *Meis2* expression in the LGE at least through *hs599*.

scATAC-seq further supported that *Dlx1/2* regulate *Meis2* expression through three enhancers

To gain further insights into the mechanism by which *Dlx1/2* regulates *Meis2* expression, we performed single-cell ATAC-seq (scATAC-seq) of the LGE at E14.5 (Fig. 7A). First, we generated an scATAC-seq dataset from 849 cells passing quality control criteria (see methods). Through integration of the promoter and gene body accessibility in scATAC-seq, we identified 7 clusters (C0-C6), including radial glial cells (C5), basal radial glial cells (C0), intermediate progenitor cells (C3), immature MSNs (C4), immature D1 MSNs (C2), D2 MSNs (C6) and D1 MSNs (C1) (Fig. 7B). The identity of cell clusters was further confirmed by assessing a set of cell-type-specific genes ascertained by differential gene expression analysis (Figs. 7C-F; Figs. S7A-C). According to chromatin accessibility changes, we constructed developmental trajectories of all cell populations (Fig. 7G). Our results suggested that D1 and D2 MSNs are derived from common progenitors. According to a recent study, the same progenitors give rise to both D1 and D2 MSNs in humans (Bocchi et al., 2021). Enhancers are often found in chromatin accessible regions where TFs preferentially bind (Nord et al., 2015). Therefore, we attempted to reveal the chromatin accessibility of the DLX1/2 binding regions near *Meis2*. Our results showed that the enhancer *hs355* and putative enhancer R1 had high chromatin accessibility in all cell populations (Figs. 7H-I). In contrast, the chromatin accessibility of the enhancer *hs599* was high in intermediate progenitor (SVZ) cells and immature MSNs but low in radial glial cells and mature MSNs (Fig. 7J). These results indicated that

hs599 might exert its function mainly in differentiating cells rather than in LGE VZ radial glia and mature MSNs. This is consistent with our above result – the expression of *Meis2* is mainly reduced in the LGE SVZ of the *hs599* mutant mice. Finally, we identified multiple loci featuring DLX binding in those regions (Figs. 7H-J), which are consistent with previous DLX ChIP-seq studies (Lindtner et al., 2019). Altogether, our findings provided strong evidence that *Dlx1/2* directly promote *Meis2* expression in the LGE through multiple enhancers.

DISCUSSION

In all studied vertebrates, there are two types of striatal MSNs (D1 and D2 MSNs) that have distinct roles in motor control, reinforcement learning, and motivation (Dudman and Krakauer, 2016; Grillner et al., 2013; Peters et al., 2021). They are derived from common LGE progenitors (Bocchi et al., 2021; Kelly et al., 2018). However, the molecular mechanisms that specify MSNs, let alone D1 versus D2 MSNs are incompletely understood. Here we found that *Meis2* plays a central role in the generation of MSNs. In *Meis2*-CKO mice, there is a block in the differentiation of LGE progenitors, resulting in the accumulation of proliferating and immature cells in an enlarged LGE (Figs. 8A-B), similar to the phenotype *of Dlx1/2* mutants (Anderson et al., 1997). Integrating of our RNA-seq, ATAC-seq and CUT&Tag-seq analyses provides evidence that *Meis2* directly regulates the expression of *Six3* and *Zfp503* to control the specification of D2 and D1 MSNs, respectively (Fig. 8C). DLX1/2 directly binds to three putative *Meis2* enhancers, including *hs599*, which are implicated in promoting *Meis2* expression (Lindtner et al., 2019; McGregor et al., 2019; Silberberg et al., 2016). We generated a deletion of *hs599*; in its absence, there is reduced *Meis2* expression in the LGE SVZ. Consistent with this, our scATAC-seq data provides evidence for *hs599* activity in the LGE intermediate SVZ progenitors. Overall, our findings provided evidence that *Meis2* promotes the fate determination of striatal MSNs by promoting *Six3* and *Zfp503* expression and that DLX1/2 drive *Meis2* expression through enhancer *hs599*.

Meis2 is a key factor for generating mature MSNs

Elucidating the transcriptional networks in the developing striatum requires the knowledge of both the cellular and developmental functions and the genome-wide molecular functions of individual TFs. Twenty years ago, the homeobox genes *Dlx1/2* were reported to be required for the generation of striatal MSNs. In its absence, the number of MSNs was greatly reduced due to a block in differentiation (Anderson et al., 1997). Subsequently, many other factors were reported to be essential for the development of striatal MSNs, such as *Gsx2*, *Ascl1*, *Ebf1* and *Isl1* (Chapman et al., 2013; Corbin et al., 2000; Corbin et al., 2003; Ehrman et al., 2013; Garel et al., 1999; Horton et al., 1999; Lobo et al., 2006; Lobo et al., 2008; Long et al., 2009b; Lu et al., 2014; Waclaw et al., 2009; Wang et al., 2013; Wang et al., 2009; Yun et al., 2002). *Meis2* is a Hox gene co-factor which is highly expressed in the LGE and its derivatives from embryonic to adult stages. CKO of *Meis2* in the LGE greatly reduced the number of striatal MSNs due to a block in differentiation (Fig. 1E and Figs. 3A-J). Recent studies have shown that the TFs *Six3* and *Zfp503* are crucial for the generation of the D2 and D1 MSNs, respectively (Chen et al., 2020; Soleilhavoup et al., 2020; Song et al., 2021; Xu et al., 2018). CUT&Tag-seq technology revealed that *Meis2* directly binds to the promoters of *Six3* and *Zfp503* (Figs. 5A-B). Consistent with this, *Six3* and *Zfp503* expressions were greatly reduced in *Meis2*-CKO mice (Fig. 5D). Therefore, our findings suggested that *Meis2* is a central factor in the specification of D1 and D2 MSNs by promoting *Zfp503* and *Six3* expressions, respectively. Thus, *Meis2* is a crucial step in determining the fate of MSN precursors on their path to become D1 or D2 MSNs. Although our previous study showed that *Meis2* was involved in striatal MSN survival (Yang et al., 2021b), this study highlighted that the mechanism by which *Meis2* regulates the development of striatal MSNs. Finally, another possible result in loss of striatal MSNs in the *Meis2*-CKO mice is that *Meis2* regulates dorsal (d) vs ventral (v) LGE identity. Because we observe the expansion of the *Sp8* expression but not the *Etv1* and *Tshz1*(not shown), we speculated that the blockage of generating striatal MSNs in the *Meis2*-CKO mice mainly due to fail to express *Zfp503* and *Six3*.

***Meis2* regulates genes involved in retinoic acid production in the LGE SVZ**

RA, a small molecule derived from vitamin A is a ligand for nuclear RA receptors, and has been proposed to play important roles in striatal neurogenesis (Berenguer and Duester, 2021; Chatzi et al., 2011; Liao et al., 2008; Oulad-Abdelghani et al., 1997; Toresson et al., 1999; Urban et al., 2010; Waclaw et al., 2004). RA is synthesized by Raldh3 (*Aldh1a3*) in LGE progenitors at E12.5 (Molotkova et al., 2007; Toresson et al., 1999), and the *Gsx2* TF is required for *Aldh1a3* expression (Waclaw et al., 2004). *Aldh1a3* is essential for the differentiation of striatal MSNs (Chatzi et al., 2011). Based on our findings, we hypothesize that *Aldh1a3* LGE expression is directly promoted by *Meis2*. The reasons are as follows: 1) RNA-seq showed that the expression of *Aldh1a3* was significantly decreased at E14.5 in *Meis2*-CKO mice. 2) ISH showed that *Aldh1a3* expression was abolished at E12.5 and E16.5. 3) CUT&Tag-seq revealed that *Meis2* directly binds to the *Aldh1a3* promoter region. 4) There were many immature neurons in the LGE SVZ of *Meis2*-CKO mice, but they did not express *Aldh1a3*. Hence, we speculate that *Aldh1a3*, at least as a part of *Meis2*, is a direct downstream target that regulates the differentiation of striatal MSNs.

Dlx1/2* regulate *Meis2* expression in the LGE SVZ through the enhancer *hs599

Our findings demonstrated that proliferating cells and immature neurons accumulated in the LGE SVZ of *Meis2*-CKO mice due to abnormal differentiation. These phenotypes are very similar to those in the LGE of *Dlx1/2* mutant mice (Anderson et al., 1997). Furthermore, the expression of *Dlx1/2* was increased in the LGE SVZ of *Meis2*-CKO mice, and the expression of *Meis2* was greatly reduced in the LGE SVZ of *Dlx1/2* mutant mice. Therefore, we hypothesize that *Dlx1/2* are upstream factors that promote *Meis2* expression in the LGE SVZ. Analysis of recently published data showed that *Dlx1/2* directly bound to three enhancer regions (*hs355*, putative enhancer region 1 and *hs599*) near *Meis2* (Lindtner et al., 2019). The luciferase assays also supported our hypothesis. Because *hs599* is active during development of the LGE (McGregor et al., 2019; Silberberg et al., 2016; Visel et al., 2013), we wondered whether *hs599* can promote *Meis2* expression. CRISPR/Cas9 genome

editing generated a deletion of *hs599*. Analysis of *hs599*$^{-/-}$ mice showed that the expression of *Meis2* was reduced in the LGE SVZ (Figs. 6E-F). Considering that an enhancer might show different activity in distinct populations of cells, we performed scATAC-seq to determine *hs599* chromatin in different populations of LGE cells at E14.5. The chromatin of enhancer *hs599* was mainly open in immature neurons (Fig. 7J). Altogether, our findings indicated that *Dlx1/2* directly regulate the expression of *Meis2* in the LGE SVZ at least partially via the enhancer *hs599*.

In sum, our findings clearly elucidated the mechanism by which *Meis2* regulates the development of striatal MSNs. This study will provide a solid theoretical basis for further research on striatum development and related diseases.

Acknowledgements

We are grateful to Kenneth Campbell at University of Cincinnati College of Medicine for the *Dlx5/6*-CIE mice.

Data availability

CUT&Tag-seq, RNA-seq and sc-ATAC-seq data have been deposited in Gene Expression Omnibus under accession number GSE114344 and GSE188602.

Competing interests

We declare that there is no conflict of interest.

Author contributions

Z.S. and Z.W. performed all experiments and analyzed data. S.L., L.Y., Z.S., Y.T., R.G., Y.Y., and W.Z. helped to conduct experiments and analyze the data. Z.Z. designed the experiments and analyzed the results. Z.Z., J.R. and Z.Y. wrote the manuscript.

Funding

This work was supported by research grants to Z. Yang from National Key Research and Development Program of China (2018YFA0108000), National Natural Science Foundation of China (NSFC 31630032 and 31820103006), Shanghai Municipal Science and Technology Major Project (2018SHZDZX01), ZJ Lab, and Shanghai Center for Brain Science and Brain-Inspired Technology, research grant to J. Rubenstein (R01 MH049428 from NIMH).

MATERIALS AND METHODS

Key resources table

Reagent or Resource	Source	Identifier
Antibodies		
Rabbit Anti-ASCL1	Cosmo Bio	SK-T01-003, Dilution: 1:2000
Rat Anti-BCL11B	Abcam	ab18465, Dilution: 1:200
Rat Anti-BrdU	Accurate Chemical and Scientific Corporation	OBT0030S, Dilution: 1:200
Rabbit Anti-CRE	Millipore	69050, Dilution: 1:1000
Rabbit Anti-DCX	Abcam	ab18723, Dilution: 1:1000
Guinea Pig Anti-DLX2	Gift from Kazuaki Yoshikawa	Dilution: 1:2000
Rabbit Anti-EBF1	Santa Cruz Biotechnology	sc-15888, Dilution: 1:500
Rabbit Anti-FOXP1	Abcam	ab16645, Dilution: 1:2000
Goat Anti-FOXP2	Abcam	ab58599, Dilution: 1:500
Chicken Anti-GFP	Aves labs	GFP-1020, Dilution: 1:2000
Rabbit Anti-GSX2	Millipore	ABN162, Dilution: 1:2000
Rabbit Anti-ISL1	Abcam	ab20670, Dilution: 1:800

Mouse Anti-MEIS2	Santa Cruz Biotechnology	sc-515470, Dilution: 1:500
Mouse Anti-PCNA	Abcam	ab29, Dilution: 1:1000
Rabbit Anti-PH3	Millipore	06-570, Dilution: 1:1500
Rabbit Anti-SP9	Our Laboratory	Dilution: 1:500
Rabbit Anti-KI67	Vector Labs	VP-K451, Dilution: 1:500
Mouse Anti- SIX3	Santa Cruz Biotechnology	sc-398797, Dilution: 1:800
Mouse Anti-TUBB3	Covance	MMS-435P, Dilution: 1:500

Experimental models

Mouse: C57BL/6	Department of laboratory Animal science at Fudan University	http://10.107.12.196/
Mouse: CD1	Department of laboratory Animal science at Fudan University	http://10.107.12.196/
Mouse: *Meis2*$^{F/+}$	This manuscript	N/A; Available from the authors
Mouse: *Six3*$^{F/+}$	Gift from Guillermo Oliver at Northwestern University	N/A; Available from the authors
Mouse: *Dlx5/6-CIE*	Gift from Kenneth Campbell at University of Cincinnati College of Medicine	N/A; Available from the authors
Mouse: *Gsx2-Cre*	The Jackson Laboratory	025806
Mouse: *Dlx1/2*$^{+/-}$	Gift from John L. Rubenstein at University of California	N/A; Available from the authors
Mouse: *Zfp503*$^{F/+}$	This manuscript	N/A; Available from the authors

Software and algorithms

Photoshop CC	Adobe Systems Incorporated	RRID: SCR_014199
Olympus VS120 digital slice scanning system	Olympus	N/A
Prism v.7	GraphPad	N/A
CellRanger v2.1.1	10X Genomics	https://www.10xgenomics.com/solutions/single-cell/
FASTQC v0.11.5	Babraham Bioinformatics	https://www.bioinformatics.babraham.ac.uk/projects/fastqc/
UMI Tools v0.5.4	（(Li et al., 2021)）	https://github.com/CGATOxford/UMI-tools

Recombinant DNA

pCAGIG	Addgene	Cat#11159
pGL4.10	Promega	Cat#E6651
pGL4.23	Promega	Cat#E8411

Deposited data

RNA-seq data	This manuscript	Not yet
ATAC-seq	This manuscript	Not yet
Single-cell ATAC-seq	This manuscript	Not yet
CUT&Tag-seq	This manuscript	Not yet

All secondary antibodies were from Jackson ImmunoResearch Labs.

Secondary Antibodies	Cat Number	Dilution Ratio
Alexa®488-conjugated Affinipure Donkey Anti-Rabbit IgG (H^+L)	711-545-152	1:500
Cy^{TM}3-conjugated Affinipure Donkey Anti-Rabbit IgG (H^+L)	711-165-152	1:500
Alexa®488-conjugated Affinipure Donkey Anti-Mouse IgG (H^+L)	715-545-151	1:500
Cy^{TM}3-conjugated Affinipure Donkey Anti-Mouse IgG (H^+L)	715-165-151	1:500
Alexa®488-conjugated Affinipure Donkey Anti-Chicken IgY^{++} (IgG) (H^+L)	703-545-155	1:500
Cy™3-AffiniPure Donkey Anti-Goat IgG (H^+L)	705-505-147	1:500
Cy™3-AffiniPure Donkey Anti-Rat IgG (H^+L)	712-165-150	1:500
Cy™3-AffiniPure Donkey Anti-Guinea Pig IgG (H^+L)	706-165-148	1:500

EXPERIMENTAL PROCEDURES

Animals

All experiments conducted in this study were in accordance with guidelines from Fudan University. *Meis2*$^{F/+}$ (Yang et al., 2021b), *Six3*$^{F/+}$ (Xu et al., 2018), *Dlx5/6-CIE* (Zhang et al., 2019), *Gsx2-Cre* (Wei et al., 2019) and *Dlx1/2*$^{+/-}$ (Anderson et al., 1997) mice were previously described. *Zfp503*$^{F/+}$ mice were generated via the CRISPR/Cas9 strategy. LoxP sites flanked the coding region of exon 3 (Figs. S6A-D). Genotyping of the *Zfp503* constitutive knockout (KO) allele was performed by PCR using the following primers:

F4: 5'-GCCACACAAACTTGTCTCCTTTT-3';

R4: 5'-CAGCACACACTCCTTGATTCTAAAG-3'; and

R5: 5’-TAAACTTTCTTTTCCCTTCCGTAGC-3’. These primers yield bands of 253 and 305 bp for the wild-type and mutant alleles, respectively. *hs599*$^{+/-}$ mice with deletion of the *hs599* enhancer were generated by CRISPR/Cas9 techniques, (Fig. 6D; Figs. S6E-H). Genotyping of the *hs599* mutant allele was performed by PCR using the following primers:

WT-F: 5’- GGAGAGATGTTGCTGCTAGTGAGGC-3’;

WT-R: 5’- CGCTTGAGTCATTAACAGTGTGCCC-3’; and

Mut-F: 5’- AACCATTAACATCTGTGAGATGCTGTC-3’. These primers yield bands of 455 and 583 bp for the wild-type and mutant alleles, respectively. All mice were maintained in a mixed genetic background of C57BL/6J and CD1. The day of vaginal plug detection was considered E0.5, and the day of birth was defined as P0. Both male and female mice were used in all experiments.

BrdU Labeling

A single intraperitoneal injection of BrdU (50mg/kg) was adiministered at E14.5 or E16.5. BrdU incorporation was analyzed 2 h after BrdU injection.

Tissue preparation

Tissue preparation was performed as previously described(Liu et al., 2018).

Immunohistochemistry

In this study, 6-μm thick frozen sections were used for immunostaining. The sections were washed with 0.05 M TBS for 10 min, incubated in Triton-X-100 (0.5% in 0.05 M TBS) for 30 min at room temperature (RT), and then incubated with blocking solution (10% donkey serum +0.5%; Triton-X-100 in 0.05 M TBS, pH= 7.2) for 2 h at RT. The primary antibodies were diluted in 10% donkey serum blocking solution, incubated overnight at 4 °C, and then rinsed 3 times with 0.05 M TBS. Secondary antibodies (from Jackson, 1:500) matching the appropriate species were added and incubated for 2-4 h at RT. Fluorescently stained sections were then washed 3 times with 0.05 M TBS. This was followed by 4’,6-diamidino-2-phenylindole (DAPI) (Sigma, 200 ng/ml)

staining for 5 min, and then the sections were then cover-slipped with Gel/Mount (Biomeda, Foster City, CA). The primary antibodies used in this study are listed in the table below:

In situ RNA hybridization

ISH was performed on 20-μm cryosections using digoxigenin riboprobes as previously described (Liu et al., 2018). Probes were made from P0 wild-type mouse brain cDNA amplified by PCR using the following primers:

Probe Name	Primer Sequence
Rarb	Primer F: AAGGGCTTTTTCCGCAGAAGTAT
	Primer R: AGCAGTGGTGACTGACTGACTCCA
Rxrg	Primer F: GGACAGATCCTCAGGGAAGCACTA
	Primer R: GCCACCTTTAACAGCCGTACAAAA
Six3	Primer F: AGAGTTGTCCATGTTCCAGTTG
	Primer R: CTGATTTCGGTTTGTTCTAGGG
Zfp503	Primer F: TCCCAGGGACAGACAAACTGCT
	Primer R: TACAAGGGATCGGAGGGTTTGTT
Meis2	Primer F: AGAGCATGCCAGGGGACTACGT
	Primer R: CTCCGCAGCATGGTTCTTTTCTC
Ikzf1	Primer F: TTGTTCACTGGTAGCTGAGGTTTCC
	Primer R: GGGAACCTGTACTGGTCACACTGTG
Gad1	Primer F: ATGGCATCTTCCACTCCTTCG
	Primer R: TTACAGATCCTGACCCAACCTCTC
Penk	Primer F: TCGGAAGGACAGGATGTCATCA
	Primer R: CGTCAGGAGAGATGAGGTAACAAAC
Dlx5	Primer F: CAGCTTTCAGCTGGCCGCTT
	Primer R: CAAGGCACCATTGATAGTGTCCACA

Aldh1a3	Primer F: GTGCTCACCAGGGAGTGTTCTTCA
	Primer R: TCTGCCTTAGATGGGCCTATGTCG
Adora2a	Primer F: ATGGGCTCCTCGGTGTACATCATG
	Primer R: TCAGGAAGGGGCAAACTCTGAAGAC
Drd2	Primer F: CGGGAGCTGGAAGCCTCGA
	Primer R: TGCAGGGTCAAGAGAAGGCCG

RNA-seq

RNA-seq analysis was performed as previously described (Liu et al., 2018). The LGEs of E14.5 *Meis2-CKO* and littermate control mice were dissected (n = 4). Gene expression levels were reported as fragments per kilobase of exon per million fragments mapped (FPKM). Genes with a p value <0.05 were considered would be called as differentially expressed.

Bulk ATAC-seq

The ATAC assay was performed using dissected E14.5 LGEs of wild-type mice and *Meis2*-CKO mice (n = 3 per group). The tissues were harvested, and the cells were counted. Then, $5x10^4$ cells were centrifuged for 5 min at 500 × g and 4 °C. The supernatant was removed and discard. The cells were washed once with 50 µl of cold PBS buffer and centrifuged for 5 min at 500 × g and 4 °C. The supernatant was removed and discard. A pipet was used to gently resuspend the cell pellet in 50 µl of cold lysis buffer (10 mM Tris·Cl, pH 7.4 (APPENDIX 2A),10 mM NaCl, 3 mM MgCl2, 0.1% (v/v) Igepal CA-630, stored up to 1 week at 4°C). The mixture was centrifuged immediately for 10 min at 500 × g and 4 °C. The supernatant was discarded, and the transposition reaction was immediately continued. The cell pellet was placed on ice. To make the transposition reaction mix, the following reagents were combined: 10 µl 5x TTBL (Vazyme TD501 kit); 5 µl TTE Mix V50 (Vazyme TD501 kit); and 35 µl nuclease-free H_2O. The nuclear pellet was resuspended in the transposition reaction mix and incubated at 37 °C for 30 min. Immediately following transposition, the

samples was purified using VAHTS DNA Cleans Beads. The transposed DNA was eluted in 25 µl ddH2O. To amplify transposed DNA fragments, the following reagents were combined in a 0.2 ml PCR tube: 24 µl transposed DNA; 10 µl 5X TAB (Vazyme TD501 kit); 5 µl PCR Primer Mix (PPM) (Vazyme TD501 kit); 5 µl P5 Primer X (Vazyme TD202 kit); 5 µl P7 Primer X (Vazyme TD202 kit); and 1 µl TAE (Vazyme TD501 kit). The reaction was performed with a thermal cycler as follows: 72 °C for 3 min; 98 °C for 30 s; 12 cycles of 98 °C for 15 s, 60 °C for 30 s and 72 °C for 30 s; 72 °C for 5 min and hold at 4 °C. To purify the PCR products, 1.2 × volumes of VAHTS DNA Clean Beads (Vazyme) were added and incubated at room temperature for 10 min. The libraries were washed twice with 80% ethanol and eluted in 22 µl of ddH2O. The libraries were sequenced on an Illumina NovaSeq platform, and 150-bp paired-end reads were generated.

scATAC-seq

Nuclei were isolated and washed according to the instructions supplied by 10X Genomics [Nuclei Isolation for Single Cell ATAC Sequencing (CG000169)]. The isolated nuclei were resuspended in chilled diluted nuclei buffer (10X Genomics; 2000153) at a volume based on the number of starting cells and the final target concentration of nuclei. A Countstar instrument (Rigel S2) was used to count the nuclei, which were immediately used to generate single-cell ATAC-seq libraries. Following the 10X Genomics instructions for the sc-ATAC solution, the Chromium Chip E Single Cell Kit (Product Code 1000156) and the Chromium Single Cell ATAC Library & Gel Bead Kit (Product Code 1000110), the nuclei in the bulk sample were partitioned into nanoliter-scale gel beads-in-emulsion; a pool of ~750,000 10^9 barcodes was sampled to separately and uniquely index the transposed DNA of each individual nucleus, and libraries were generated (by CapitalBio Technology, Beijing). The libraries were sequenced using an Illumina Nova-seq sequencer with a sequencing depth of at least 25,000 read pairs per nucleus with a paired-end 50-bp reading strategy. The Cell Ranger ATAC 1.2.0 pipeline and the mm10 reference genome were downloaded from the 10X Genomics website

(https://support.10xgenomics.com/single-cell-atac/software/downloads/latest). Raw sequencing data were converted to fastq format using cell rangeratac mkfastq.6806 cells. Cells with pct_reads_in_peaks >40, peak_region_fragments >3,000 and <80,000, TSS.enrichment >2.5, blacklist_ratio <0.01, and nucleosome_signal <4 were also filtered out. Peak calling, peak annotation, clustering visualization, TF motif enrichment analysis, and differential accessibility analysis were performed with the Signac package (https://satijalab.org/signac/index.html). We generated an scATAC-Seq dataset from 1219 cells passing quality control criteria from 4 embryos of 1 litter. Next, we removed the striatal interneurons (markers: *Nkx2.1*, *Lhx6* and *Sst*), septum neurons (markers: *Zic1, Zic2* and *Zic4*) and cortical projection neurons (*Tbr1*, *Pax6* and *Neurod1*) according to the mRNA expression profile. We finally obtained 849 cells. Dimensionality was reduced using Latent Semantic Indexing (LSI), and the top 2–30 principal components were used to generate clusters by calculating k-nearest neighbors and constructing the shared nearest neighbor (SNN) graph, which was visualized via UMAP.

For analysis of cell lineages trajectory, we used a cell lineage inference algorithm, Slingshot (version 1.2.0, https://bioconductor.org/packages/slingshot/), to predict lineage trajectories and bifurcations by ordering cells along trajectories. Slingshot takes as input a matrix of gene activity from Signac. Lineages are defined by ordered sets of clusters beginning with the root node and terminating in the most distal cluster(s) with only one connection. Potential fitting curves are drawn to the subsets of cells that potentially make up each lineage. The ordering provided by Slingshot, analogous to pseudo-developmental time points, is referred to here as developmental order. The cluster representing radial glial cells (RGCs) was chosen as the starting root node. The most variable genes among all single cells were identified by Seurat. A pseudo-developmental timeline of single cells was calculated with the Slingshot package, using the most variable genes as time-ordering genes. We mainly used the Signac package code:

library(Signac)

```
library(Seurat)
library(GenomeInfoDb)
library(EnsDb.Mmusculus.v79)
library(ggplot2)
library(patchwork)
library(dplyr)
set.seed(1234)
counts <- Read10X_h5(filename = ".../filtered_peak_bc_matrix.h5")
metadata <- read.csv(file = ".../singlecell.csv",header = TRUE, row.names = 1)
chrom_assay <- CreateChromatinAssay(counts = counts,sep = c(":", "-"),genome =
'mm10', fragments = '.../fragments.tsv.gz', min.cells = 1)
pbmc <- CreateSeuratObject(counts = chrom_assay, assay = "peaks", meta.data =
metadata)
annotations <- GetGRangesFromEnsDb(ensdb = EnsDb.Mmusculus.v79)
seqlevelsStyle(annotations) <- 'UCSC' genome(annotations) <- "mm10"
Annotation(pbmc) <- annotations
pbmc <- NucleosomeSignal(object = pbmc)
pbmc <- TSSEnrichment(object = pbmc, fast = FALSE)
pbmc$pct_reads_in_peaks <- pbmc$peak_region_fragments / pbmc$passed_filters *
100
pbmc$blacklist_ratio <- pbmc$blacklist_region_fragments /
pbmc$peak_region_fragments
pbmc$high.tss <- ifelse(pbmc$TSS.enrichment > 2, 'High', 'Low')
TSSPlot(pbmc, group.by = 'high.tss') + NoLegend()
pbmc$nucleosome_group <- ifelse(pbmc$nucleosome_signal > 4, 'NS > 4', 'NS < 4')
FragmentHistogram(object = pbmc, group.by = 'nucleosome_group')
pbmc <- subset(x = pbmc, subset = peak_region_fragments > 3000
&peak_region_fragments < 80000 &pct_reads_in_peaks > 40 &blacklist_ratio < 0.01
& nucleosome_signal < 4 & TSS.enrichment > 2.5)
pbmc <- RunTFIDF(pbmc)
```

pbmc <- FindTopFeatures(pbmc, min.cutoff = 'q0')

pbmc <- RunSVD(pbmc)

pbmc <- RunUMAP(object = pbmc, reduction = 'lsi', dims = c(2:50))

pbmc <- FindNeighbors(object = pbmc, reduction = 'lsi', dims = c(2:50))

pbmc <- FindClusters(object = pbmc, verbose = FALSE, algorithm = 3,resolution = 1)

gene.activities <- GeneActivity(pbmc)

pbmc[['ATAC']] <- CreateAssayObject(counts = gene.activities)

pbmc <- NormalizeData(object = pbmc,assay = 'ATAC',normalization.method = 'LogNormalize', scale.factor = 10000)

CUT&Tag-seq

The CUT&Tag assay was performed using E14.5 LGEs dissected from wild-type CD1 mice and a MEIS2 mouse polyclonal antibody as described previously. Briefly, the cells were isolated from the LGE. Then, $1x10^5$ cells were washed with 500 µl of wash buffer (10× wash buffer (-), 50× protease inhibitor cocktail, ddH_2O) and centrifuged at 600 rcf for 3 min at RT. The cell pellets were resuspended in 100 µl of wash buffer. Concanavalin A-coated magnetic beads were washed twice with binding buffer (10× binding buffer, ddH_2O). Next, 10 µl of activated beads were added and incubated at RT for 10 min. Bead-bound cells were resuspended in 50 µl of antibody buffer (10× wash buffer (-), 50× protease inhibitor cocktail, ddH_2O, 5% digitonin, 0.5 M EDTA, 30% BSA). Then, 1 µg of primary antibody (mouse polyclonal anti-MEIS2 antibody, Santa Cruz Biotechnology) or nothing was added and incubated at RT for 2 h. The primary antibody was removed using a magnet stand. Secondary antibody (1 µg, goat anti-mouse) was diluted in 50 µl of Dig-wash buffer (10× wash buffer (-), 50× Protease inhibitor cocktail, ddH_2O, 5% digitonin), and cells were incubated at room temperature for 1 h. Cells were washed three times with Dig-wash buffer to remove unbound antibodies. The Hyperactive pG-Tn5 Transposase adaptor complex (TTE mix, 4 µM, Vazyme) was diluted 1:100 in 100 µl of Dig-300 buffer (10× Dig-300 buffer (-), 5% digitonin, 50× protease inhibitor cocktail, ddH_2O). The cells were incubated with 0.04 µM TTE mix at room temperature for 1 h. The cells were washed three times with

Dig-300 buffer to remove unbound TTE mix. Then, the cells were then resuspended in 300 µl of tagmentation buffer (10 mM $MgCl_2$ in Dig-300 buffer) and incubated at 37 °C for 1 h. To terminate tagmentation, 10 µl of 0.5 M EDTA, 3 µl of 10% SDS and 2.5 µl of 20 mg ml^{-1} Proteinase K were added to 300 µl of sample and incubated overnight at 37 °C. DNA was purified using phenol-chloroform-isoamyl alcohol extraction and ethanol precipitation with RNase A treatment. For library amplification, 24 µl of DNA was mixed with 1 µl of TruePrep Amplify Enzyme (TAE, Vazyme), 10 µl of 5× TruePrep Amplify Enzyme Buffer and 5 µl of ddH_2O, and 5 µl of uniquely barcoded i5 and i7 primers from TruePrep Index Kit V2 for Illumina (Vazyme). A total of 50 µl of sample was placed in a thermocycler and subjected to the following program: 72 °C for 3 min; 98 °C for 30 s; 17 cycles of 98 °C for 15 s, 60 °C for 30 s and 72 °C for 30 s; 72 °C for 5 min and hold at 4 °C. To purify the PCR products, 1.2× volumes of VAHTS DNA Clean Beads (Vazyme) were added and incubated at RT for 10 min. The libraries were washed twice with 80% ethanol and eluted in 22 µl of ddH2O. The libraries were sequenced on an Illumina NovaSeq platform, and 150-bp paired-end reads were generated.

All raw sequence data were quality trimmed to a minimum Phred score of 20 using Trimmomatic. Apparent PCR duplicates were removed using Picard MarkDuplicates vl.107. All reads produced by CUT&Tag of MEIS2 were aligned to the mm10 mouse genome using Bowtie2 version 2.3.4. Sequence tags were aligned to the genome and then subsequently analyzed by MACS2 software version 2.1.4 to detect genomic regions enriched for multiple overlapping DNA fragments (peaks) that we considered to be putative binding sites. Peaks with a false discovery rate lower than 5% were saved to detect chromosomal regions for further analyses. Visualization of peak distribution along genomic regions of genes of interest was performed with the Integrative Genomics Viewer (IGV).

Dual-luciferase assays

The DNA fragments of the *hs355*, *hs599* and R1 enhancers near the *Meis2* gene were created by PCR and subsequently cloned into the pGL4.23 firefly luciferase vector (Promega) upstream of the Luc2 gene. Cells from the mouse embryonal carcinoma cell line N2a were grown in medium MEMa (Gibco, 12571063) supplemented with 10% fetal bovine serum (FBS) (Gibco, 10099141). For the luciferase assay, N2a cell transfections were performed in triplicate in 24-well plates by using Fugene HD transfection reagent according to the manufacturer's protocol (Promega, E2311). Luciferase activity was quantified by a microplate luminometer (Turner BioSystems, Modulus microplate reader).

The primers used for amplifying the putative Meis2 enhancers were as follows:

hs599 Fwd: 5' -AGCAACATCTCTCCAAGCCACCTGT-3';

hs599 Rev: 5'-TCAGGGACCACCTTCTTGACACCGA-3';

hs355 Fwd: 5' -GCACCTCTTTGTACACAGATATTTAAACATGGC-3';

hs355 Rev: 5'-ATACGCACAGAGGTCATTTCAAAAACCCTTATAG-3';

R1 Fwd: 5' -AAGCACTCCAGCCTGAATCCACAGTCCTCAGGAT-3'; and

R1 Rev: 5'-CCCAAGCTTGTTCTGTACTCCTTCAGGGTTTACAGGGA-3'.

The *Six3* promoter and *Zfp503* promoter were amplified by PCR and cloned into the pGL4.10 firefly luciferase vector (Promega) upstream (U) of the Luc2 gene. The primers used for amplifying the putative promoter were as follows:

Six3 promoter 1: Fwd:5'- TTCTGTTTCGCCCTCTTCTCCCTC-3';

Rev:5'-TGGAAAGGAGGGGGGAGCAGAAG-3';

Six3 promoter 2: Fwd: 5'-CACTGTGGATTTAGGGGAGATATTATG-3';

Rev: 5'-AGGAGGAAGGACGTAAGGGACA-3';

Zfp503 promoter: Fwd:5'-AGGCCTTTGGGCTGGCCTGGGTTCCT-3';

Rev:5'-CCCCTCCTCCGCCTCTCAGCCACTCT-3';

Image acquisition and statistical analysis

Images for quantitative analyses were acquired with an Olympus VS 120 microscope using a 20X objective. Bright field images were acquired with an Olympus VS 120 microscope using a 10X objective. Images were merged, cropped and optimized in Adobe Photoshop CC without distorting the original information. Analyses were performed using GraphPad Prism 6.0, Microsoft Excel and R language. Unpaired t test was used to determine statistical significance. All quantification results are presented as the mean ± SEM. Differences with *p* values < 0.05 were considered significant. For quantification of $GSX2^+$, $ASCL1^+$, $PCNA^+$, $DLX2^+$, CRE^+ (DLX5/6), $SP9^+$ and $SP8^+$ cells in the LGE SVZ at E16.5, four anatomically matched 6-μm thick coronal sections were selected (n = 4 mice per group). We counted $GSX2^+$, $ASCL1^+$, $PCNA^+$, $DLX2^+$, CRE^+ (DLX5/6), $SP8^+$ and $SP9^+$ cells in the LGE SVZ under a 20X objective lens. The LGE SVZ was delineated by DAPI staining. The data of $GSX2^+$, $ASCL1^+$, $PCNA^+$, $DLX2^+$, CRE^+ (DLX5/6), $SP9^+$ and $SP8^+$ cells per section for each LGE SVZ were presented as the relative ratio of the control group.

For quantification of $TUBB3^+$, DCX^+ and $MEIS2^+$ cells in the LGE SVZ at E16.5, four anatomically matched 6-μm thick coronal sections were selected (n = 4 mice per group). We used the histogram tool in Adobe Photoshop CC to calculate the fluorescence intensity of $TUBB3^+$ and DCX^+ in the LGE SVZ. And data were presented in proportion to the control group. For quantitative analysis of in situ hybridization with *Gad1* probes, the *Gad1* signal intensity in the LGE SVZ was analyzed using the Image J software.

For quantification of $Sp8^+$, CB^+, TH^+, and $Pax6^+$ cells in the control and *Meis2*-CKO mice, 20μm sections from OB were analyzed. 2-5 random regions(500×500 pix) per OB section and 4 sections per animal were counted using 20X objective on an Olympus VS120 microscope. We analyzed 4 mice per group.

For quantification of FOXP1$^+$, MEIS2$^+$ and FOXP1/MEIS2 double positive cells in the mouse striatum at P30, four 20-μm thick coronal sections from rostral, intermediate, and caudal levels of the striatum were selected (n = 4 mice per group). We used ImageJ to count the number of FOXP1$^+$, MEIS2$^+$ and FOXP1/MEIS2 double positive cells in each striatum. Brain regions were identified using a mouse brain atlas, and sections equivalent to the following bregma coordinates were taken (in mm): the most-rostral section, 1.18; and the most- caudal section, −0.10. For quantification of KI67$^+$, PH3$^+$ and BrdU$^+$ cells in the mouse LGE SVZ at E16.5, four anatomically matched 10-μm thick coronal sections were selected (n = 4 mice per group). We counted KI67$^+$, PH3$^+$ and BrdU$^+$ cells in the LGE SVZ under a 20X objective lens. The LGE SVZ was delineated by DAPI staining.

References

Anderson, S. A., Qiu, M., Bulfone, A., Eisenstat, D. D., Meneses, J., Pedersen, R. and Rubenstein, J. L. (1997). Mutations of the homeobox genes Dlx-1 and Dlx-2 disrupt the striatal subventricular zone and differentiation of late born striatal neurons. *Neuron* **19**, 27-37.http://dx.doi.org/10.1016/s0896-6273(00)80345-1

Arlotta, P., Molyneaux, B. J., Jabaudon, D., Yoshida, Y. and Macklis, J. D. (2008). Ctip2 controls the differentiation of medium spiny neurons and the establishment of the cellular architecture of the striatum. *J Neurosci* **28**, 622-632.http://dx.doi.org/10.1523/JNEUROSCI.2986-07.2008

Berenguer, M. and Duester, G. (2021). Role of Retinoic Acid Signaling, FGF Signaling and Meis Genes in Control of Limb Development. *Biomolecules* **11**.http://dx.doi.org/10.3390/biom11010080

Bocchi, V. D., Conforti, P., Vezzoli, E., Besusso, D., Cappadona, C., Lischetti, T., Galimberti, M., Ranzani, V., Bonnal, R. J. P., De Simone, M., et al. (2021). The coding and long noncoding single-cell atlas of the developing human fetal striatum. *Science* **372**.http://dx.doi.org/10.1126/science.abf5759

Castro, D. S., Martynoga, B., Parras, C., Ramesh, V., Pacary, E., Johnston, C., Drechsel, D., Lebel-Potter, M., Garcia, L. G., Hunt, C., et al. (2011). A novel function of the proneural factor Ascl1 in progenitor proliferation identified by genome-wide characterization of its targets. *Genes Dev* **25**, 930-945.http://dx.doi.org/10.1101/gad.627811

Chapman, H., Waclaw, R. R., Pei, Z., Nakafuku, M. and Campbell, K. (2013). The homeobox gene Gsx2 controls the timing of oligodendroglial fate specification in mouse lateral ganglionic eminence progenitors. *Development* **140**, 2289-2298.http://dx.doi.org/10.1242/dev.091090

Chatzi, C., Brade, T. and Duester, G. (2011). Retinoic acid functions as a key GABAergic differentiation signal in the basal ganglia. *PLoS Biol* **9**, e1000609.http://dx.doi.org/10.1371/journal.pbio.1000609

Chen, S. Y., Lu, K. M., Ko, H. A., Huang, T. H., Hao, J. H., Yan, Y. T., Chang, S. L., Evans, S. M. and Liu, F. C. (2020). Parcellation of the striatal complex into dorsal and ventral districts. *Proc Natl Acad Sci U S A*.http://dx.doi.org/10.1073/pnas.1921007117

Corbin, J. G., Gaiano, N., Machold, R. P., Langston, A. and Fishell, G. (2000). The Gsh2 homeodomain gene controls multiple aspects of telencephalic development. *Development* **127**, 5007-5020

Corbin, J. G., Rutlin, M., Gaiano, N. and Fishell, G. (2003). Combinatorial function of the homeodomain proteins Nkx2.1 and Gsh2 in ventral telencephalic patterning. *Development* **130**, 4895-4906.http://dx.doi.org/10.1242/dev.00717

Cunningham, T. J. and Duester, G. (2015). Mechanisms of retinoic acid signalling and its roles in organ and limb development. *Nat Rev Mol Cell Biol* **16**, 110-123.http://dx.doi.org/10.1038/nrm3932

Doyle, J. P., Dougherty, J. D., Heiman, M., Schmidt, E. F., Stevens, T. R., Ma, G., Bupp, S., Shrestha, P., Shah, R. D., Doughty, M. L., et al. (2008). Application of a translational profiling approach for the comparative analysis of CNS cell types. *Cell* **135**, 749-762.http://dx.doi.org/10.1016/j.cell.2008.10.029

Dudman, J. T. and Krakauer, J. W. (2016). The basal ganglia: from motor commands to the control of vigor. *Curr Opin Neurobiol* **37**, 158-166.http://dx.doi.org/10.1016/j.conb.2016.02.005

Ehrman, L. A., Mu, X., Waclaw, R. R., Yoshida, Y., Vorhees, C. V., Klein, W. H. and Campbell, K. (2013). The LIM homeobox gene Isl1 is required for the correct development of the striatonigral pathway in the mouse. *Proc Natl Acad Sci U S A* **110**, E4026-4035.http://dx.doi.org/10.1073/pnas.1308275110

Fazel Darbandi, S., Poitras, L., Monis, S., Lindtner, S., Yu, M., Hatch, G., Rubenstein, J. L. and Ekker, M. (2016). Functional consequences of I56ii Dlx enhancer deletion in the developing mouse forebrain. *Dev Biol*.http://dx.doi.org/10.1016/j.ydbio.2016.10.015

Garel, S., Marin, F., Grosschedl, R. and Charnay, P. (1999). Ebf1 controls early cell differentiation in the embryonic striatum. *Development* **126**, 5285-5294

Gehring, W. J., Affolter, M. and Burglin, T. (1994). Homeodomain proteins. *Annu Rev Biochem* **63**, 487-526.http://dx.doi.org/10.1146/annurev.bi.63.070194.002415

Gerfen, C. R., Engber, T. M., Mahan, L. C., Susel, Z., Chase, T. N., Monsma, F. J., Jr. and Sibley, D. R. (1990). D1 and D2 dopamine receptor-regulated gene expression of striatonigral and striatopallidal neurons. *Science* **250**, 1429-1432.http://dx.doi.org/10.1126/science.2147780

Gerfen, C. R. and Surmeier, D. J. (2011). Modulation of striatal projection systems by dopamine. *Annu Rev Neurosci* **34**, 441-466.http://dx.doi.org/10.1146/annurev-neuro-061010-113641

Giliberti, A., Curro, A., Papa, F. T., Frullanti, E., Ariani, F., Coriolani, G., Grosso, S., Renieri, A. and Mari, F. (2020). MEIS2 gene is responsible for intellectual disability, cardiac defects and a distinct facial phenotype. *Eur J Med Genet* **63**, 103627.http://dx.doi.org/10.1016/j.ejmg.2019.01.017

Gokce, O., Stanley, G. M., Treutlein, B., Neff, N. F., Camp, J. G., Malenka, R. C., Rothwell, P. E., Fuccillo, M. V., Sudhof, T. C. and Quake, S. R. (2016). Cellular Taxonomy of the Mouse Striatum as Revealed by Single-Cell RNA-Seq. *Cell Rep* **16**, 1126-1137.http://dx.doi.org/10.1016/j.celrep.2016.06.059

Golonzhka, O., Nord, A., Tang, Paul L. F., Lindtner, S., Ypsilanti, Athena R., Ferretti, E., Visel, A., Selleri, L. and Rubenstein, John L. R. (2015). Pbx Regulates Patterning of the Cerebral Cortex in Progenitors and Postmitotic Neurons. *Neuron* **88**, 1192-1207.http://dx.doi.org/10.1016/j.neuron.2015.10.045

Grillner, S., Robertson, B. and Stephenson-Jones, M. (2013). The evolutionary origin of the vertebrate basal ganglia and its role in action selection. *Journal of Physiology-London* **591**, 5425-5431.http://dx.doi.org/10.1113/jphysiol.2012.246660

Hikida, T., Kimura, K., Wada, N., Funabiki, K. and Nakanishi, S. (2010). Distinct roles of synaptic transmission in direct and indirect striatal pathways to reward and aversive behavior. *Neuron* **66**, 896-907.http://dx.doi.org/10.1016/j.neuron.2010.05.011

Hintiryan, H., Foster, N. N., Bowman, I., Bay, M., Song, M. Y., Gou, L., Yamashita, S., Bienkowski, M. S., Zingg, B., Zhu, M., et al. (2016). The mouse cortico-striatal projectome. *Nature Neuroscience* **19**, 1100-1114.http://dx.doi.org/10.1038/nn.4332

Horton, S., Meredith, A., Richardson, J. A. and Johnson, J. E. (1999). Correct coordination of neuronal differentiation events in ventral forebrain requires the bHLH factor MASH1. *Mol Cell Neurosci* **14**, 355-369.http://dx.doi.org/10.1006/mcne.1999.0791

Kelly, S. M., Raudales, R., He, M., Lee, J. H., Kim, Y., Gibb, L. G., Wu, P., Matho, K., Osten, P., Graybiel, A. M., et al. (2018). Radial Glial Lineage Progression and Differential Intermediate Progenitor Amplification Underlie Striatal Compartments and Circuit Organization. *Neuron* **99**, 345-361 e344.http://dx.doi.org/10.1016/j.neuron.2018.06.021

Larsen, K. B., Lutterodt, M. C., Laursen, H., Graem, N., Pakkenberg, B., Mollgard, K. and Moller, M. (2010). Spatiotemporal distribution of PAX6 and MEIS2 expression and total cell numbers in the ganglionic eminence in the early developing human forebrain. *Dev Neurosci* **32**, 149-162.http://dx.doi.org/10.1159/000297602

Li, J., Wang, C., Zhang, Z., Wen, Y., An, L., Liang, Q., Xu, Z., Wei, S., Li, W., Guo, T., et al. (2017). Transcription Factors Sp8 and Sp9 Coordinately Regulate Olfactory Bulb Interneuron Development. *Cereb Cortex*, 1-17.http://dx.doi.org/10.1093/cercor/bhx199

Li, X., Liu, G., Yang, L., Li, Z., Zhang, Z., Xu, Z., Cai, Y., Du, H., Su, Z., Wang, Z., et al. (2021). Decoding Cortical Glial Cell Development. *Neurosci Bull*.http://dx.doi.org/10.1007/s12264-021-00640-9

Liao, W. L., Tsai, H. C., Wang, H. F., Chang, J., Lu, K. M., Wu, H. L., Lee, Y. C., Tsai, T. F., Takahashi, H., Wagner, M., et al. (2008). Modular patterning of structure and function of the striatum by retinoid receptor signaling. *Proc Natl Acad Sci U S A* **105**, 6765-6770.http://dx.doi.org/10.1073/pnas.0802109105

Lindtner, S., Catta-Preta, R., Tian, H., Su-Feher, L., Price, J. D., Dickel, D. E., Greiner, V., Silberberg, S. N., McKinsey, G. L., McManus, M. T., et al. (2019). Genomic Resolution of DLX-Orchestrated Transcriptional Circuits Driving Development of Forebrain GABAergic Neurons. *Cell Reports* **28**, 2048-2063.e2048.http://dx.doi.org/10.1016/j.celrep.2019.07.022

Liu, J. K., Ghattas, I., Liu, S. Y., Chen, S. and Rubenstein, J. L. R. (1997). Dlx genes encode DNA-binding proteins that are expressed in an overlapping and sequential pattern during basal ganglia differentiation. *Dev Dynam* **210**, 498-512.http://dx.doi.org/Doi 10.1002/(Sici)1097-0177(199712)210:4<498::Aid-Aja12>3.0.Co;2-3

Liu, Z., Zhang, Z., Lindtner, S., Li, Z., Xu, Z., Wei, S., Liang, Q., Wen, Y., Tao, G., You, Y., et al. (2018). Sp9 Regulates Medial Ganglionic Eminence-Derived Cortical Interneuron Development. *Cerebral Cortex*.http://dx.doi.org/10.1093/cercor/bhy133

Lobo, M. K., Karsten, S. L., Gray, M., Geschwind, D. H. and Yang, X. W. (2006). FACS-array profiling of striatal projection neuron subtypes in juvenile and adult mouse brains. *Nat Neurosci* **9**, 443-452.http://dx.doi.org/10.1038/nn1654

Lobo, M. K., Yeh, C. and Yang, X. W. (2008). Pivotal role of early B-cell factor 1 in development of striatonigral medium spiny neurons in the matrix compartment. *J Neurosci Res* **86**, 2134-2146.http://dx.doi.org/10.1002/jnr.21666

Long, J. E., Cobos, I., Potter, G. B. and Rubenstein, J. L. (2009a). Dlx1&2 and Mash1 transcription factors control MGE and CGE patterning and differentiation through parallel and overlapping pathways. *Cereb Cortex* **19 Suppl 1**, i96-106.http://dx.doi.org/10.1093/cercor/bhp045

Long, J. E., Swan, C., Liang, W. S., Cobos, I., Potter, G. B. and Rubenstein, J. L. (2009b). Dlx1&2 and Mash1 transcription factors control striatal patterning and differentiation through parallel and overlapping pathways. *J Comp Neurol* **512**, 556-572.http://dx.doi.org/10.1002/cne.21854

Lu, K. M., Evans, S. M., Hirano, S. and Liu, F. C. (2014). Dual role for Islet-1 in promoting striatonigral and repressing striatopallidal genetic programs to specify striatonigral cell identity. *Proc Natl Acad Sci U S A* **111**, E168-177.http://dx.doi.org/10.1073/pnas.1319138111

Machon, O., Masek, J., Machonova, O., Krauss, S. and Kozmik, Z. (2015). Meis2 is essential for cranial and cardiac neural crest development. *BMC Dev Biol* **15**, 40.http://dx.doi.org/10.1186/s12861-015-0093-6

McGregor, M. M., McKinsey, G. L., Girasole, A. E., Bair-Marshall, C. J., Rubenstein, J. L. R. and Nelson, A. B. (2019). Functionally Distinct Connectivity of Developmentally Targeted Striosome Neurons. *Cell Rep* **29**, 1419-1428 e1415.http://dx.doi.org/10.1016/j.celrep.2019.09.076

Moens, C. B. and Selleri, L. (2006). Hox cofactors in vertebrate development. *Developmental Biology* **291**, 193-206.http://dx.doi.org/10.1016/j.ydbio.2005.10.032

Molotkova, N., Molotkov, A. and Duester, G. (2007). Role of retinoic acid during forebrain development begins late when Raldh3 generates retinoic acid in the ventral subventricular zone. *Dev Biol* **303**, 601-610.http://dx.doi.org/10.1016/j.ydbio.2006.11.035

Mukherjee, K. and Burglin, T. R. (2007). Comprehensive analysis of animal TALE homeobox genes: new conserved motifs and cases of accelerated evolution. *J Mol Evol* **65**, 137-153.http://dx.doi.org/10.1007/s00239-006-0023-0

Nord, A. S., Pattabiraman, K., Visel, A. and Rubenstein, J. L. (2015). Genomic perspectives of transcriptional regulation in forebrain development. *Neuron* **85**, 27-47.http://dx.doi.org/10.1016/j.neuron.2014.11.011

Oulad-Abdelghani, M., Chazaud, C., Bouillet, P., Sapin, V., Chambon, P. and Dollé, P. (1997). Meis2, a novel mouse Pbx-related homeobox gene induced by retinoic acid during differentiation of P19 embryonal carcinoma cells. *Dev Dyn* **210**, 173-183.http://dx.doi.org/10.1002/(sici)1097-0177(199710)210:2<173::Aid-aja9>3.0.Co;2-d

Paige, S. L., Thomas, S., Stoick-Cooper, C. L., Wang, H., Maves, L., Sandstrom, R., Pabon, L., Reinecke, H., Pratt, G., Keller, G., et al. (2012). A temporal chromatin signature in human embryonic stem cells identifies regulators of cardiac development. *Cell* **151**, 221-232.http://dx.doi.org/10.1016/j.cell.2012.08.027

Pei, Z., Wang, B., Chen, G., Nagao, M., Nakafuku, M. and Campbell, K. (2011). Homeobox genes Gsx1 and Gsx2 differentially regulate telencephalic progenitor maturation. *Proceedings of the National Academy of Sciences* **108**, 1675-1680.http://dx.doi.org/10.1073/pnas.1008824108

Peters, A. J., Fabre, J. M. J., Steinmetz, N. A., Harris, K. D. and Carandini, M. (2021). Striatal activity topographically reflects cortical activity. *Nature*.http://dx.doi.org/10.1038/s41586-020-03166-8

Silberberg, S. N., Taher, L., Lindtner, S., Sandberg, M., Nord, A. S., Vogt, D., McKinsey, G. L., Hoch, R., Pattabiraman, K., Zhang, D., et al. (2016). Subpallial Enhancer Transgenic Lines: a Data and Tool Resource to Study Transcriptional Regulation of GABAergic Cell Fate. *Neuron* **92**, 59-74.http://dx.doi.org/10.1016/j.neuron.2016.09.027

Soleilhavoup, C., Travaglio, M., Patrick, K., Garcao, P., Boobalan, E., Adolfs, Y., Spriggs, R. V., Moles-Garcia, E., Dhiraj, D., Oosterveen, T., et al. (2020). Nolz1 expression is required in dopaminergic axon guidance and striatal innervation. *Nat Commun* **11**, 3111.http://dx.doi.org/10.1038/s41467-020-16947-6

Song, X., Chen, H., Shang, Z., Du, H., Li, Z., Wen, Y., Liu, G., Qi, D., You, Y., Yang, Z., et al. (2021). Homeobox Gene Six3 is Required for the Differentiation of D2-Type Medium Spiny Neurons. *Neurosci Bull* **37**, 985-998.http://dx.doi.org/10.1007/s12264-021-00698-5

Stanley, G., Gokce, O., Malenka, R. C., Südhof, T. C. and Quake, S. R. (2019). Continuous and Discrete Neuron Types of the Adult Murine Striatum. *Neuron*.http://dx.doi.org/10.1016/j.neuron.2019.11.004

Toresson, H., Mata de Urquiza, A., Fagerstrom, C., Perlmann, T. and Campbell, K. (1999). Retinoids are produced by glia in the lateral ganglionic eminence and regulate striatal neuron differentiation. *Development* **126**, 1317-1326

Urban, N., Martin-Ibanez, R., Herranz, C., Esgleas, M., Crespo, E., Pardo, M., Crespo-Enriquez, I., Mendez-Gomez, H. R., Waclaw, R., Chatzi, C., et al. (2010). Nolz1 promotes striatal neurogenesis through the regulation of retinoic acid signaling. *Neural Dev* **5**, 21.http://dx.doi.org/10.1186/1749-8104-5-21

Valjent, E. and Gangarossa, G. (2020). The Tail of the Striatum: From Anatomy to Connectivity and Function. *Trends Neurosci*.http://dx.doi.org/10.1016/j.tins.2020.10.016

van Rhijn, J.-R., Fisher, S. E., Vernes, S. C. and Nadif Kasri, N. (2018). Foxp2 loss of function increases striatal direct pathway inhibition via increased GABA release. *Brain Structure and Function*.http://dx.doi.org/10.1007/s00429-018-1746-6

Verheije, R., Kupchik, G. S., Isidor, B., Kroes, H. Y., Lynch, S. A., Hawkes, L., Hempel, M., Gelb, B. D., Ghoumid, J., D'Amours, G., et al. (2019). Heterozygous loss-of-function variants of MEIS2 cause a triad of palatal defects, congenital heart defects, and intellectual disability. *Eur J Hum Genet* **27**, 278-290.http://dx.doi.org/10.1038/s41431-018-0281-5

Visel, A., Taher, L., Girgis, H., May, D., Golonzhka, O., Hoch, R. V., McKinsey, G. L., Pattabiraman, K., Silberberg, S. N., Blow, M. J., et al. (2013). A high-resolution enhancer atlas of the developing telencephalon. *Cell* **152**, 895-908.http://dx.doi.org/10.1016/j.cell.2012.12.041

Waclaw, R. R., Allen, Z. J., 2nd, Bell, S. M., Erdelyi, F., Szabo, G., Potter, S. S. and Campbell, K. (2006). The zinc finger transcription factor Sp8 regulates the generation and diversity of olfactory bulb interneurons. *Neuron* **49**, 503-516.http://dx.doi.org/10.1016/j.neuron.2006.01.018

Waclaw, R. R., Wang, B. and Campbell, K. (2004). The homeobox gene Gsh2 is required for retinoid production in the embryonic mouse telencephalon. *Development* **131**, 4013-4020.http://dx.doi.org/10.1242/dev.01272

Waclaw, R. R., Wang, B., Pei, Z., Ehrman, L. A. and Campbell, K. (2009). Distinct temporal requirements for the homeobox gene Gsx2 in specifying striatal and olfactory bulb neuronal fates. *Neuron* **63**, 451-465.http://dx.doi.org/10.1016/j.neuron.2009.07.015

Wang, B., Long, J. E., Flandin, P., Pla, R., Waclaw, R. R., Campbell, K. and Rubenstein, J. L. R. (2013). Loss of Gsx1 and Gsx2 function rescues distinct phenotypes in Dlx1/2 mutants. *Journal of Comparative Neurology* **521**, 1561-1584.http://dx.doi.org/10.1002/cne.23242

Wang, B., Lufkin, T. and Rubenstein, J. L. (2011). Dlx6 regulates molecular properties of the striatum and central nucleus of the amygdala. *J Comp Neurol* **519**, 2320-2334.http://dx.doi.org/10.1002/cne.22618

Wang, B., Waclaw, R. R., Allen, Z. J., 2nd, Guillemot, F. and Campbell, K. (2009). Ascl1 is a required downstream effector of Gsx gene function in the embryonic mouse telencephalon. *Neural Dev* **4**, 5.http://dx.doi.org/10.1186/1749-8104-4-5

Wang, L., Tang, Q., Xu, J., Li, H., Yang, T., Li, L., Machon, O., Hu, T. and Chen, Y. (2020). The transcriptional regulator MEIS2 sets up the ground state for palatal osteogenesis in mice. *Journal of Biological Chemistry* **295**, 5449-5460.http://dx.doi.org/10.1074/jbc.RA120.012684

Wei, S., Du, H., Li, Z., Tao, G., Xu, Z., Song, X., Shang, Z., Su, Z., Chen, H., Wen, Y., et al. (2019). Transcription factors Sp8 and Sp9 regulate the development of caudal ganglionic eminence-derived cortical interneurons. *J Comp Neurol*.http://dx.doi.org/10.1002/cne.24712

Wen, Y., Su, Z., Wang, Z., Yang, L., Liu, G., Shang, Z., Duan, Y., Du, H., Li, Z., You, Y., et al. (2021). Transcription Factor VAX1 Regulates the Regional Specification of the Subpallium Through Repressing Gsx2. *Molecular Neurobiology* **58**, 3729-3744.http://dx.doi.org/10.1007/s12035-021-02378-x

Xiao, X., Deng, H., Furlan, A., Yang, T., Zhang, X., Hwang, G.-R., Tucciarone, J., Wu, P., He, M., Palaniswamy, R., et al. (2020). A Genetically Defined Compartmentalized Striatal Direct Pathway for Negative Reinforcement. *Cell*.http://dx.doi.org/10.1016/j.cell.2020.08.032

Xu, Z., Liang, Q., Song, X., Zhang, Z., Lindtner, S., Li, Z., Wen, Y., Liu, G., Guo, T., Qi, D., et al. (2018). Sp8 and Sp9 coordinately promote D2-type medium spiny neuron production by activating Six3 expression. *Development*.http://dx.doi.org/10.1242/dev.165456

Yang, L., Li, Z., Liu, G., Li, X. and Yang, Z. (2021a). Developmental Origins of Human Cortical Oligodendrocytes and Astrocytes. *Neuroscience Bulletin*.http://dx.doi.org/10.1007/s12264-021-00759-9

Yang, L., Su, Z., Wang, Z., Li, Z., Shang, Z., Du, H., Liu, G., Qi, D., Yang, Z., Xu, Z., et al. (2021b). Transcriptional profiling reveals the transcription factor networks regulating the survival of striatal neurons. *Cell death & disease* **12**, 262-262.http://dx.doi.org/10.1038/s41419-021-03552-8

Yun, K., Fischman, S., Johnson, J., Hrabe de Angelis, M., Weinmaster, G. and Rubenstein, J. L. (2002). Modulation of the notch signaling by Mash1 and Dlx1/2 regulates sequential specification and differentiation of progenitor cell types in the subcortical telencephalon. *Development* **129**, 5029-5040

Yun, K., Potter, S. and Rubenstein, J. L. (2001). Gsh2 and Pax6 play complementary roles in dorsoventral patterning of the mammalian telencephalon. *Development* **128**, 193-205

Zha, Y., Xia, Y., Ding, J., Choi, J. H., Yang, L., Dong, Z., Yan, C., Huang, S. and Ding, H. F. (2014). MEIS2 is essential for neuroblastoma cell survival and proliferation by transcriptional control of M-phase progression. *Cell Death Dis* **5**, e1417.http://dx.doi.org/10.1038/cddis.2014.370

Zhang, Q., Zhang, Y., Wang, C., Xu, Z., Liang, Q., An, L., Li, J., Liu, Z., You, Y., He, M., et al. (2016). The Zinc Finger Transcription Factor Sp9 Is Required for the Development of Striatopallidal Projection Neurons. *Cell Rep* **16**, 1431-1444.http://dx.doi.org/10.1016/j.celrep.2016.06.090

Zhang, Y., Liu, G., Guo, T., Liang, X. G., Du, H., Yang, L., Bhaduri, A., Li, X., Xu, Z., Zhang, Z., et al. (2020). Cortical Neural Stem Cell Lineage Progression Is Regulated by Extrinsic Signaling Molecule Sonic Hedgehog. *Cell Reports* **30**, 4490-4504.e4494.http://dx.doi.org/10.1016/j.celrep.2020.03.027

Zhang, Z., Wei, S., Du, H., Su, Z., Wen, Y., Shang, Z., Song, X., Xu, Z., You, Y. and Yang, Z. (2019). Zfhx3 is required for the differentiation of late born D1-type medium spiny neurons. *Exp Neurol*, 113055.http://dx.doi.org/10.1016/j.expneurol.2019.113055

Figures

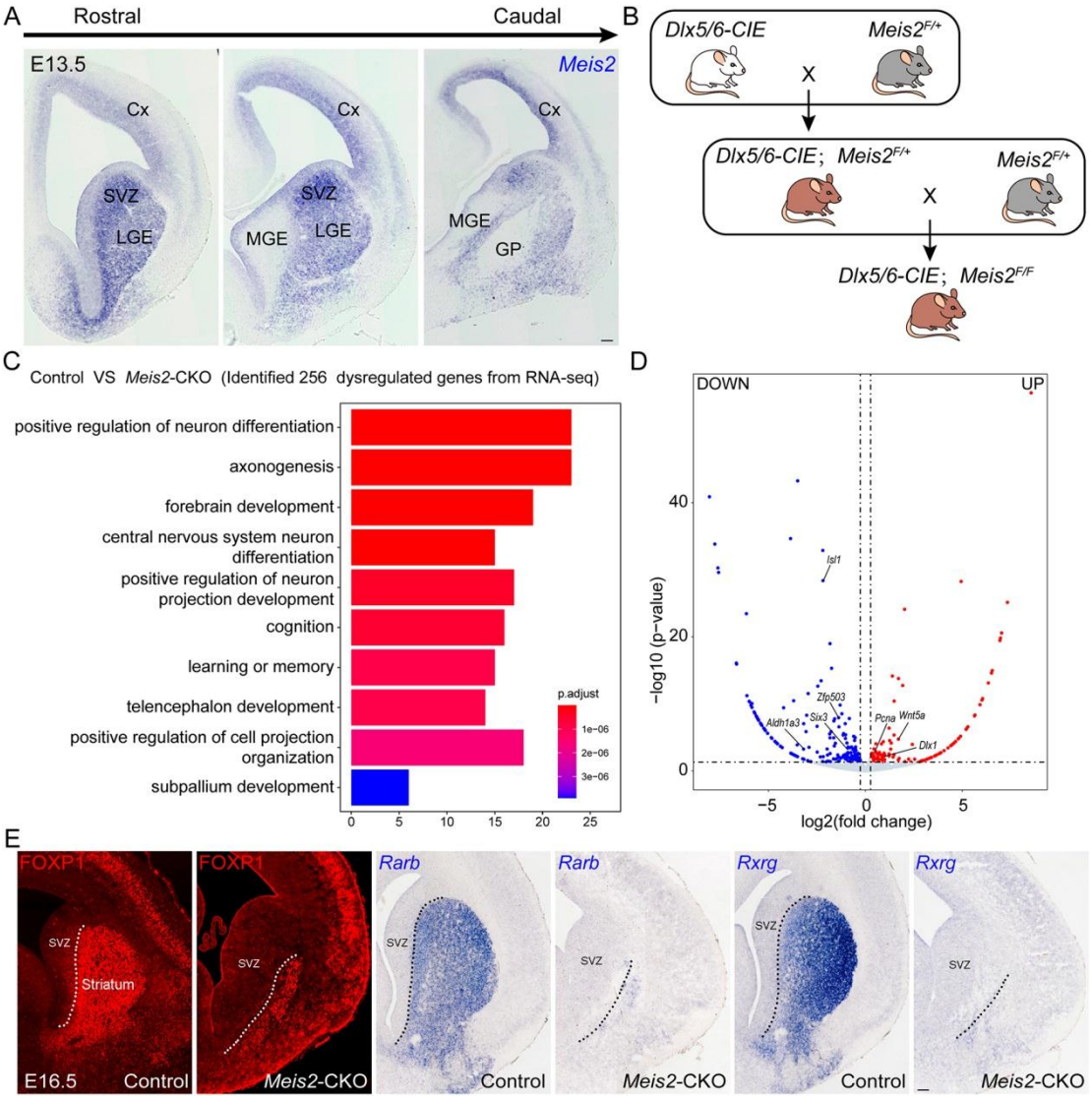

Fig. 1: The majority of striatal MSNs are lost in *Meis2*-CKO mice

(A) *Meis2* mRNA expression in a series of rostral to caudal sections at E13.5. Its expression is strongest in the LGE and septal progenitors and neurons (striatal primordium) and is remarkably low in the MGE and its derivatives. (B-C) Functional enrichment analysis of DE genes in the LGE of *Meis2*-CKO versus control mice at E14.5. (D) Volcano plots show the differentially expressed (DE) genes in the LGE at E14.5 between control and *Meis2*-CKO mice. (E) The expression of FOXP1, *Rarb* and *Rxrg* (three pan-neuronal

markers of the MSNs) was significantly decreased in *Meis2*-CKO mice compared to control mice at E16.5. Dotted lines mark the border of the LGE SVZ and striatum. Subventricular zone: SVZ. N = 4 mice per group, Scale bar: 100 μm for E.

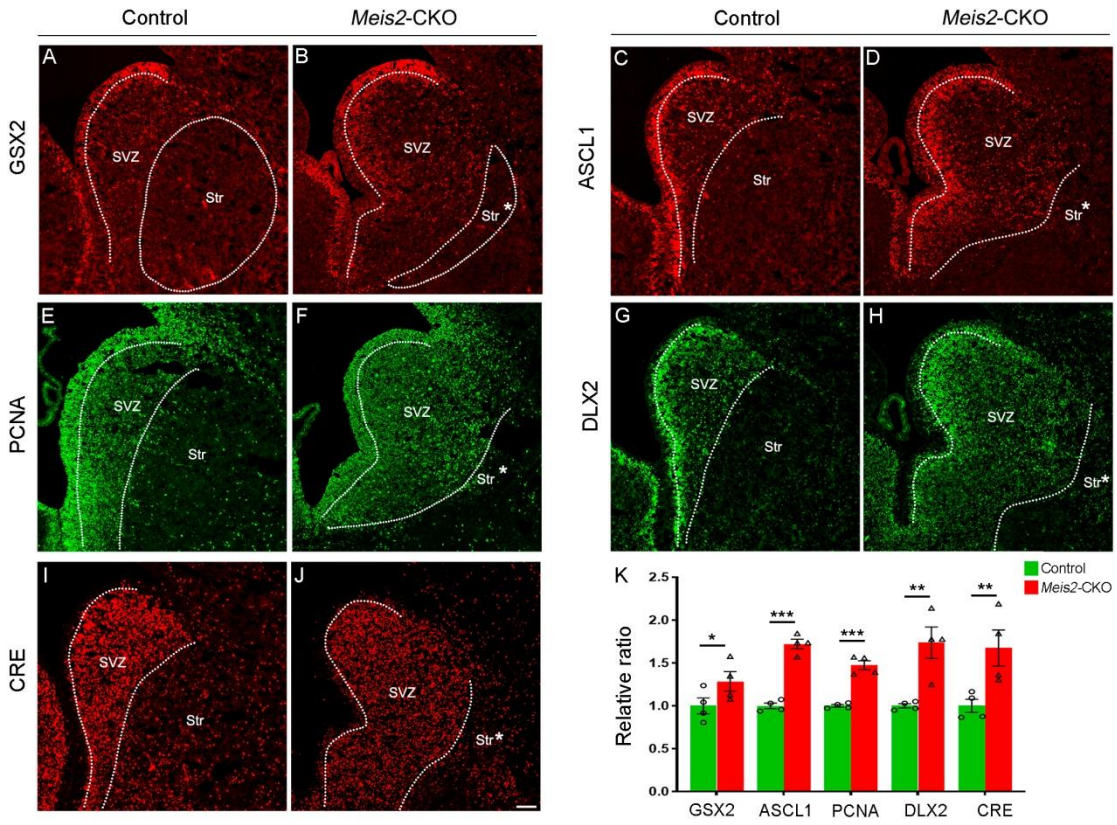

Fig. 2: Neural progenitors accumulate in the LGE SVZ of *Meis2*-CKO mice

(A-F) The number of cells expressing VZ and SVZ markers, GSX2, ASCL1 and PCNA, were increased in a greatly expanded SVZ of *Meis2*-CKO mice at E16.5. Note that the MZ was smaller in *Meis2*-CKO mice than in control mice. (G-J) Likewise, the number of cells expressing SVZ and neuronal markers, DLX2 and CRE (*Dlx5/6*), were greatly increased in SVZ of the *Meis2*-CKO mice at E16.5. (K) The number of GSX2-, ASCL1-, PCNA-, DLX2- and CRE (*Dlx5/6*) -positive cells was significantly increased in *Meis2*-CKO mice compared to control mice. (one-way ANOVA followed by Tukey–Kramer post-hoc test, *P < 0.05, **P <0 .01, ***P < 0.001, n = 4 mice per group, mean ± SEM). Dotted lines mark the border of the LGE SVZ and striatum. Subventricular zone: SVZ; Str: Striatum; Str *: presumptive striatum. Scale bar: 200 µm in J for A-J.

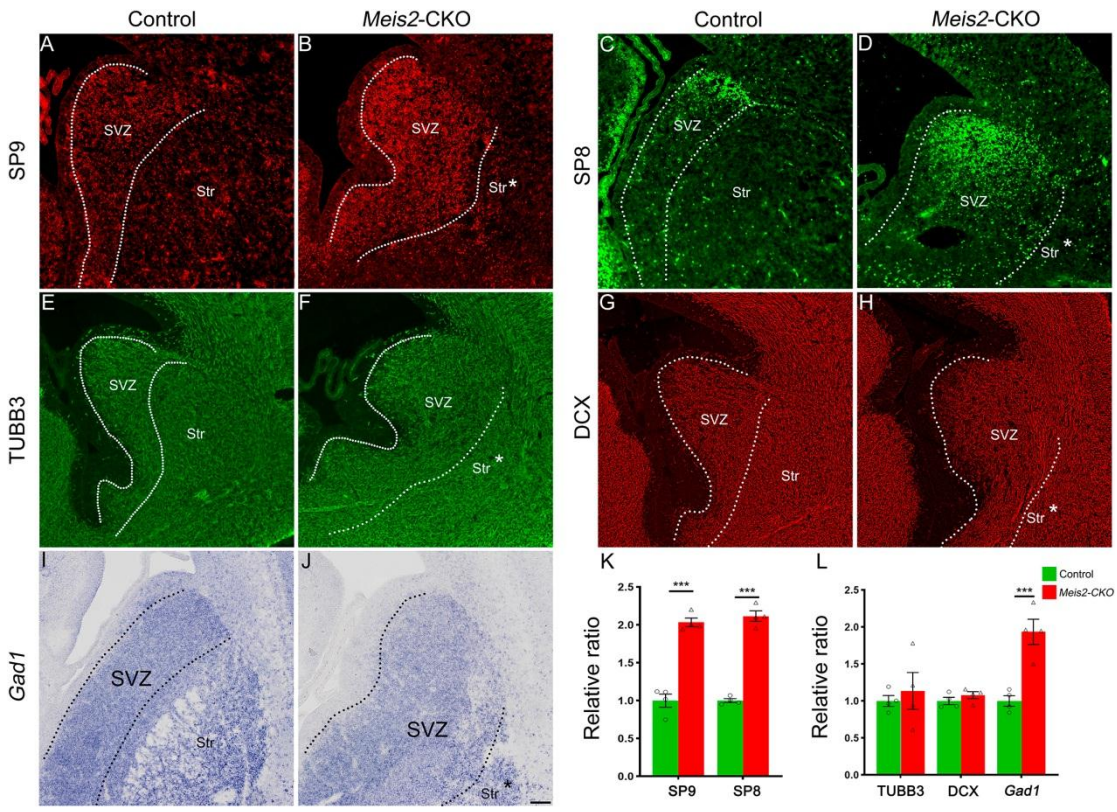

Fig. 3: The abnormal differentiation MSNs accumulate in the LGE SVZ of *Meis2*-CKO Mice

(A-D) The expression of the transcription factors SP8/9 are increased in the LGE SVZ of the *Meis2*-CKO mice compared to the controls. (E-H) There are many immature neurons which express the pan-neuronal markers TUBB3 and DCX located in the LGE SVZ of *Meis2*-CKO and control mice. (I-J) The expression of the *Gad1* is increased in the LGE SVZ of the *Meis2*-CKO mice compared to the controls. (K-L) The quantification data of the above markers in the LGE SVZ. (one-way ANOVA followed by Tukey–Kramer post-hoc test, ***P < 0.001, n = 4 mice per group, mean ± SEM). Dotted lines mark the border of the LGE SVZ and striatum. Subventricular zone: SVZ; Str: Striatum; Str *: presumptive striatum. Scale bar: 200 μm in J for A-J.

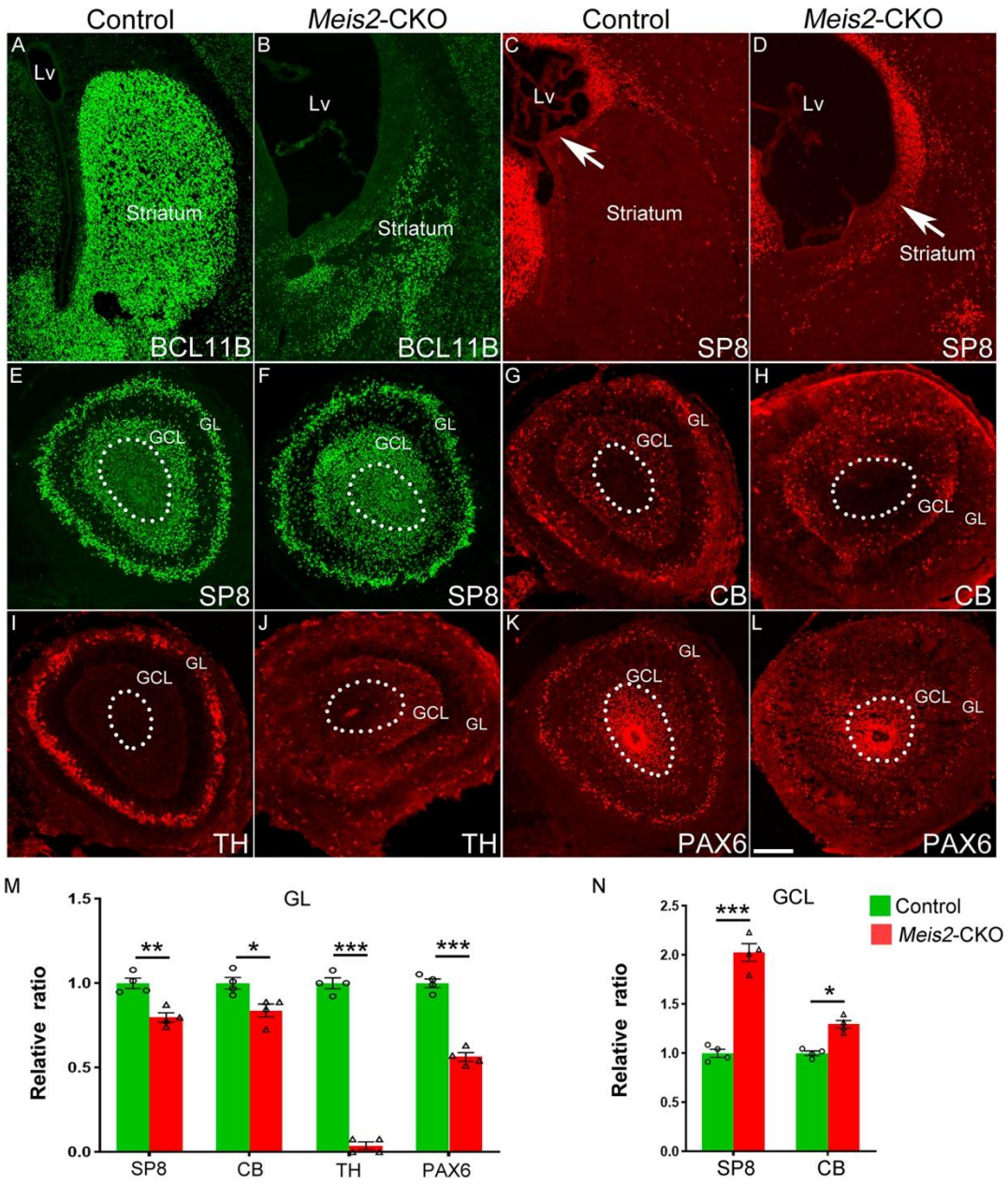

Fig. 4: *Meis2* is required for the development of OB interneurons

(A-B) Compared to controls, the number of BCL11B-positive cells was reduced in *Meis2*-CKO mice at P0 in the striatum. (C-D) More SP8-positive cells were observed in the LGE SVZ of *Meis2*-CKO mice (arrows). (E-H) The cell number of the SP8 and CB-positive cells were increased in the GCL and decreased in the GL. (I-J) There was a severe reduction of TH-positive cells in the GL of the *Meis2*-CKO mice at P0. (K-L) The expression of the PAX6 was significantly reduced in the GL. (M-N) Quantification of above experiments. (one-way ANOVA followed by Tukey–Kramer post-hoc test, *P

< 0.05, **P <0 .01, ***P < 0.001, n = 4 mice per group, mean ± SEM). Dotted lines mark the border of the OB core. GCL: Granule cell layer; GL: Glomerular layer. Scale bar: 200 µm in L for A-L.

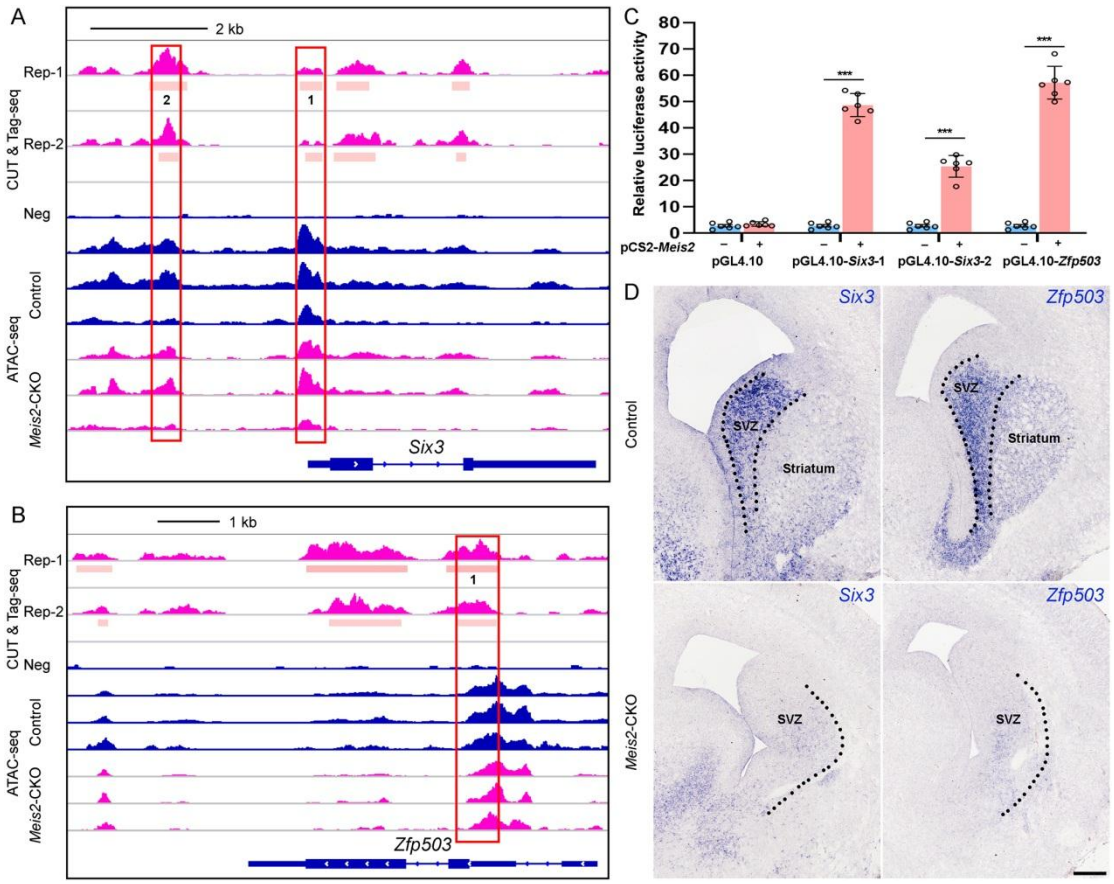

Fig. 5: *Meis2* is required for the differentiation of striatal MSNs

(A-B) Genomic regions of the *Six3* and *Zfp503* loci in the CUT&Tag-seq and ATAC-seq datasets. (C) MEIS2-activated transcription from the *Six3* and *Zfp503* promoters in a dual-luciferase assay of N2a cells. (Student's t-test, ***P < 0.001, n = 6, mean ± SEM). (D) In situ RNA hybridization analysis of *Six3* and *Zfp503* in control and *Meis2*-CKO mice at E16.5. Dotted lines mark the border of the LGE SVZ and striatum. Scale bar: 200 µm for D.

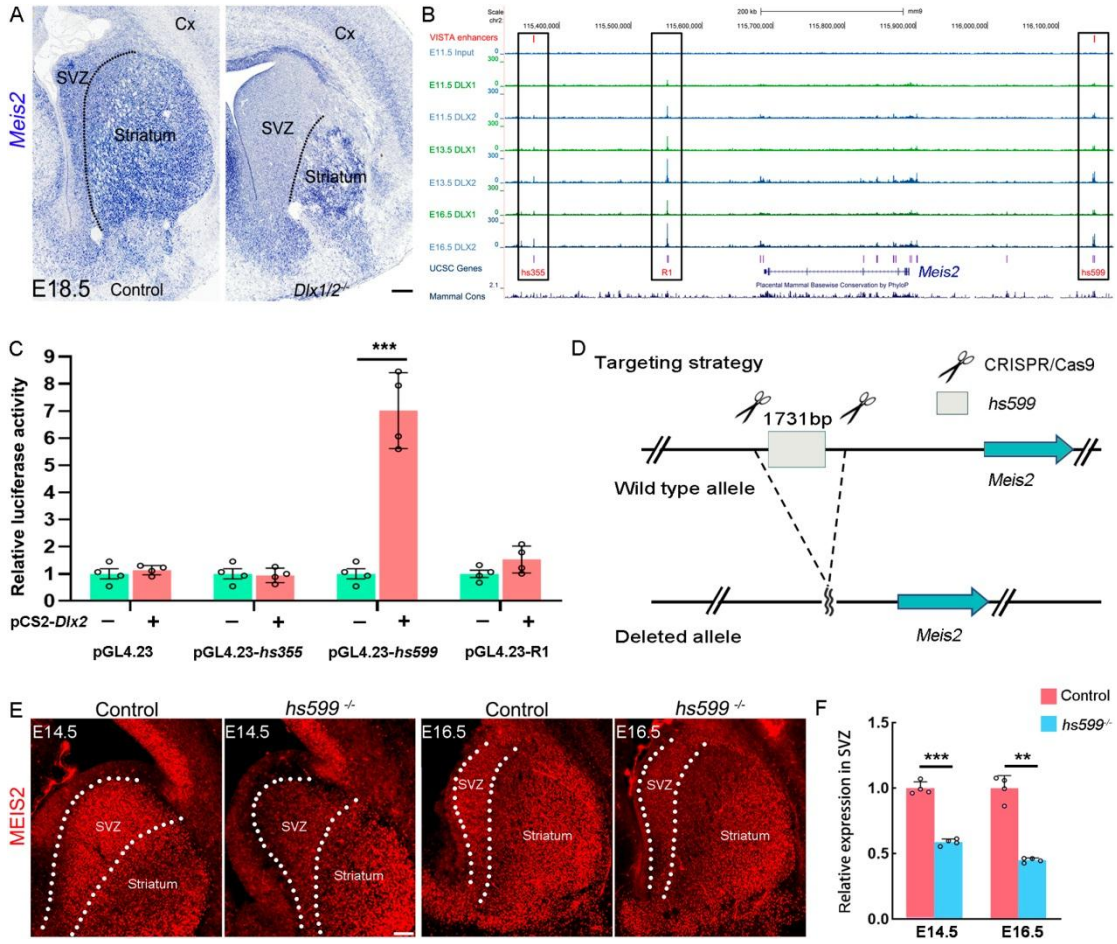

Fig. 6: *Dlx1/2* directly binds *hs599* to promote *Meis2* expression

(A) *Meis2* expression was greatly reduced in the LGE SVZ of *Dlx1/2* mutant mice. (B) DLX1/2 ChIP-seq showed that DLX1/2 directly bound to three distal regions near the *Meis2* gene. (C) The dual-luciferase assay showed that DLX1/2 promoted the activity of *hs599* (Student's t-test, **P <0 .01, ***P <0 .001, n = 4, mean ± SEM). (D) The CRISPR/Cas9 strategy was used to generate the *hs599* mutant allele. (E-F) *Meis2* expression was reduced in the LGE SVZ of the *hs599* mutant mice at E14.5 and E16.5. N = 4 mice per group. Dotted lines mark the border of the LGE SVZ and striatum. Scale bar: 200 μm in A for A; 100 μm in E for E.

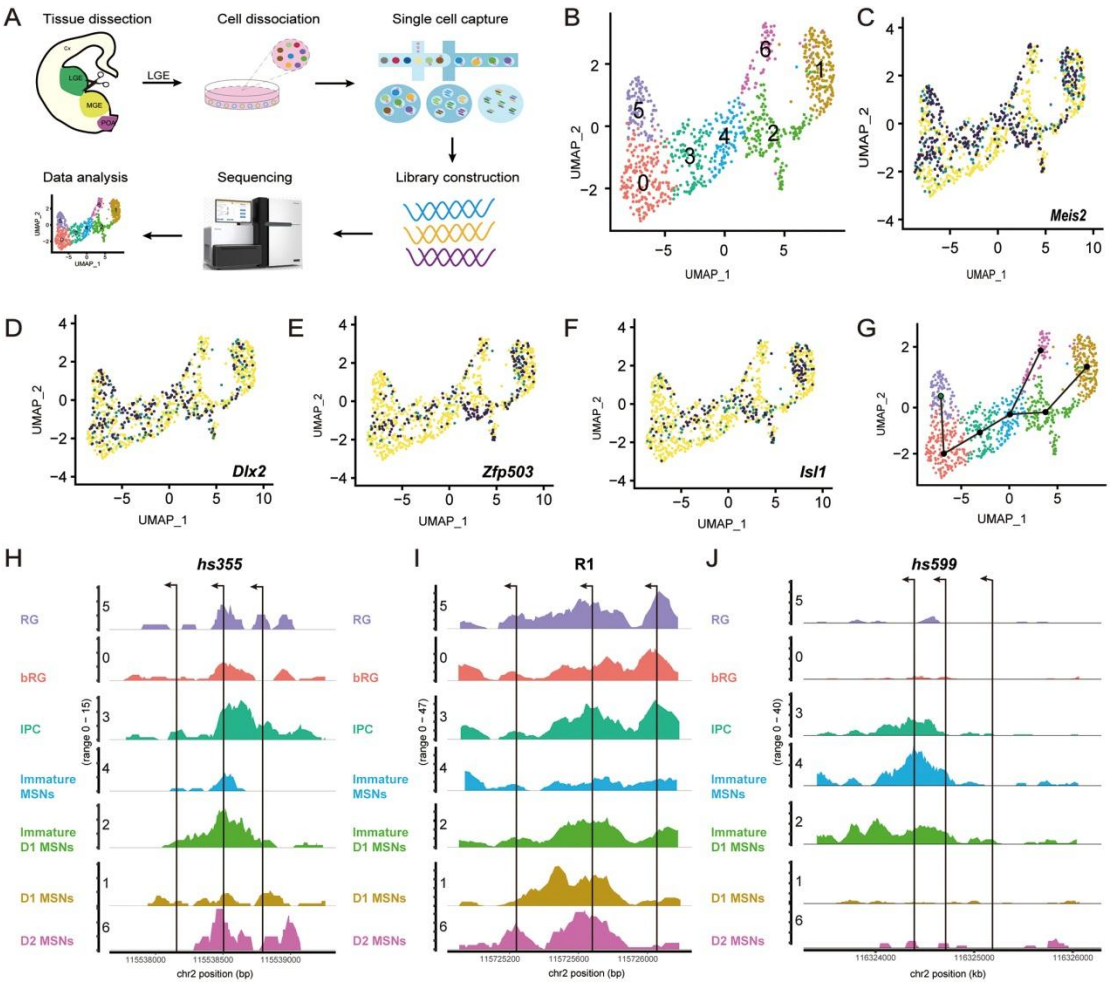

Fig. 7: scATAC-seq revealed that *hs599* exerted its function in a subpopulation of striatal MSNs

(A) Workflow of sc-ATAC-seq of mouse LGE at E14.5. (B) Seven clusters (C0-C6) were identified and annotated according to marker gene accessibility. (C-F) UMAP plots show distinct chromatin accessibility profiles of marker genes. (G) The developmental trajectory construction scheme. (H-J) Genome tracks show normalized accessibility of three DLX1/2 binding regions with cluster specific accessibility. Arrows represent the binding sites of DLX1/2.

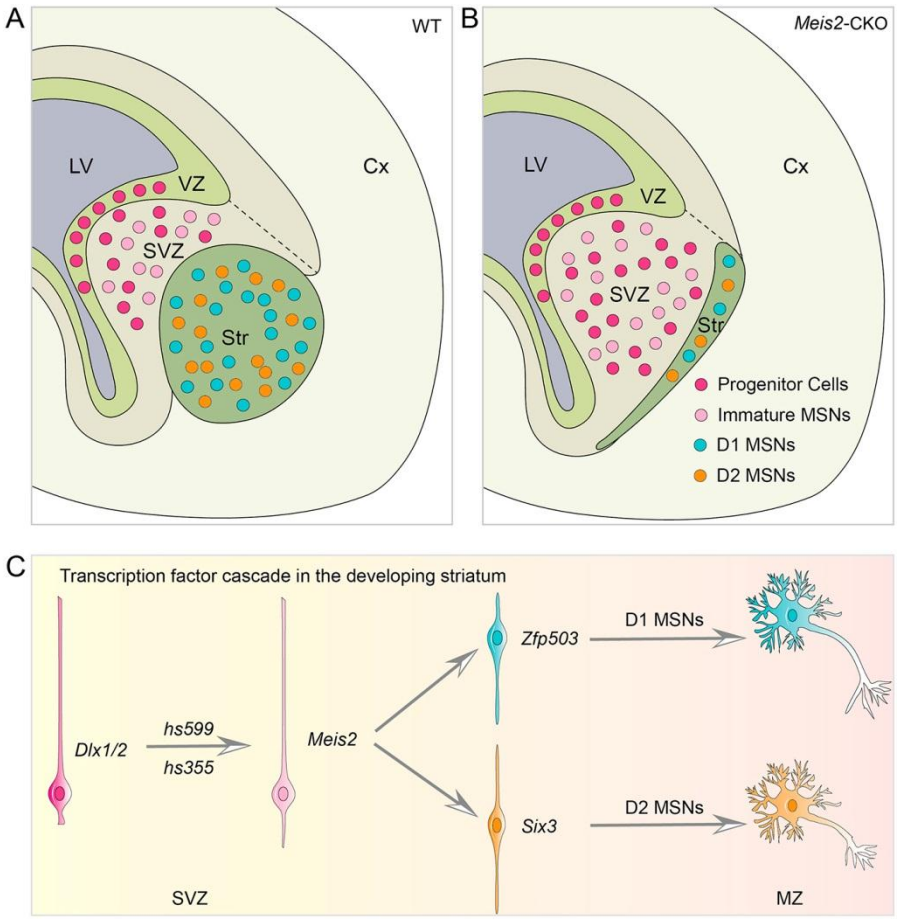

Fig. 8: A model of the mechanism by which *Meis2* regulates striatal MSN development

(A-B) Proliferating and immature cells accumulated in the LGE SVZ in *Meis2*-CKO mice, compared to control mice. Notable, the *Meis2*-CKO mice have an enlarged SVZ and a small striatum. (C) The main TF network regulating the fate determination of striatal MSNs. First, *Dlx1/2* promote the expression of *Meis2* by enhancers such as *hs599* and *hs355*. Then, *Meis2* promotes *Zfp503* or *Six3* expression to further determine precursor cell fate (D1 or D2 MSNs).

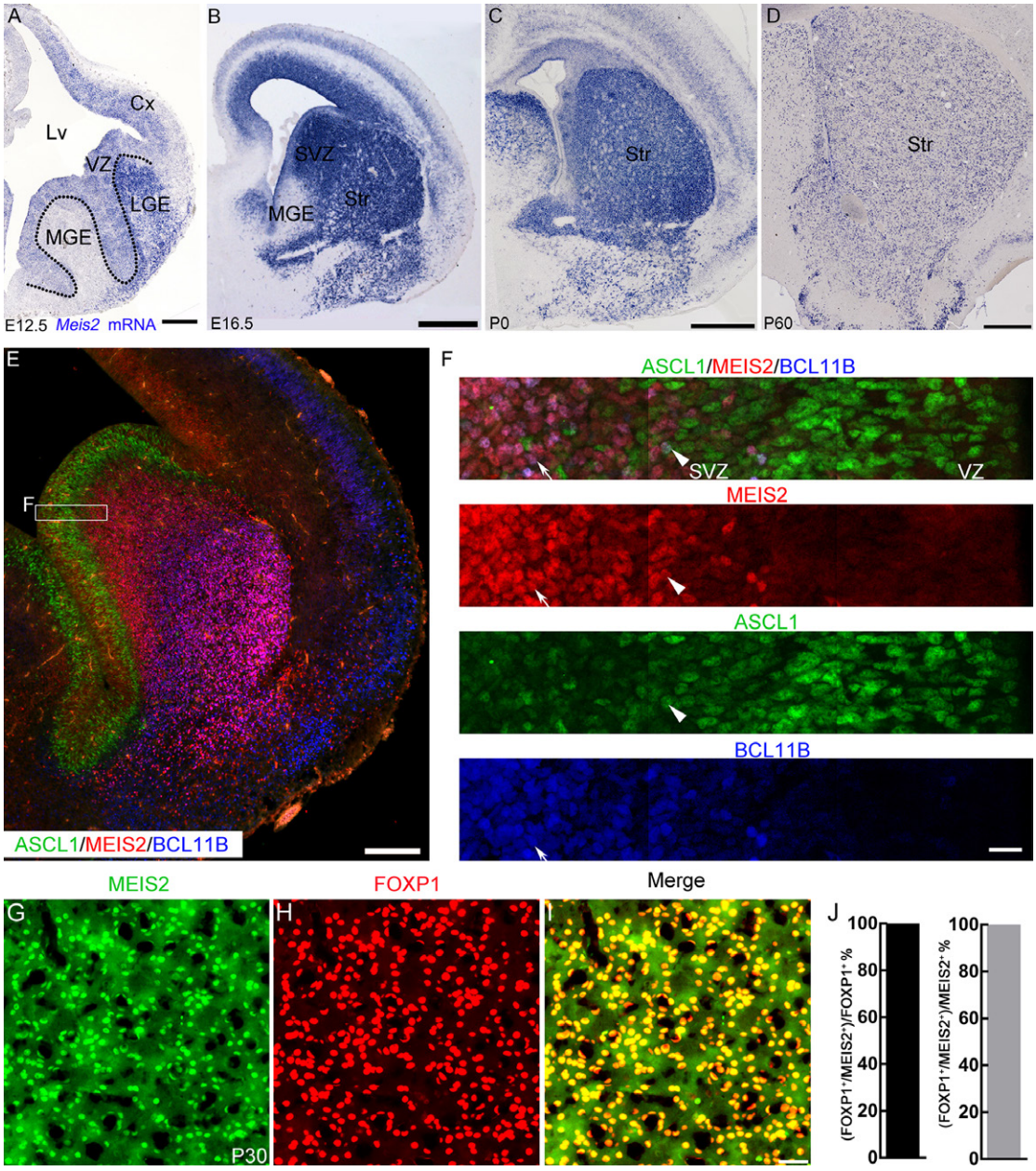

Fig. S1. *Meis2* is strongly expressed in the MSNs from early embryonic to adult stage

(A) At the early stage of E12.5, *Meis2* is strongly expressed in the LGE SVZ and relatively weakly expressed in the MGE, LGE, and cortical VZ. (B-D) ISH showed that *Meis2* was highly expressed in the whole striatum from the embryonic to adult stage. (E) ASCL1/MEIS2/BCL11B triple immunostaining coronal hemi-sections at E14.5. (F)

High magnification images of the boxed regions in E. Very few ASCL1-positive cells were co-labelled with MEIS2 (arrowhead), and the majority of BCL11B-positive cells were co-labelled with MEIS2 (arrow). (G-J) All FOXP1-positive cells were co-labelled with MEIS2 in the striatum at P30, and vice versa. Abbreviations: Cx (cortex); Lv (lateral ventricle); LGE (lateral ganglionic eminence); MGE (medial ganglionic eminence); VZ (ventricular zone); SVZ (subventricular zone); Str (striatum). Scale bars: 100 µm in A; 200 µm in B; 200 µm in C; 500 µm in D; 200 µm in E; 100 µm in F; 100 µm in I for G-I.

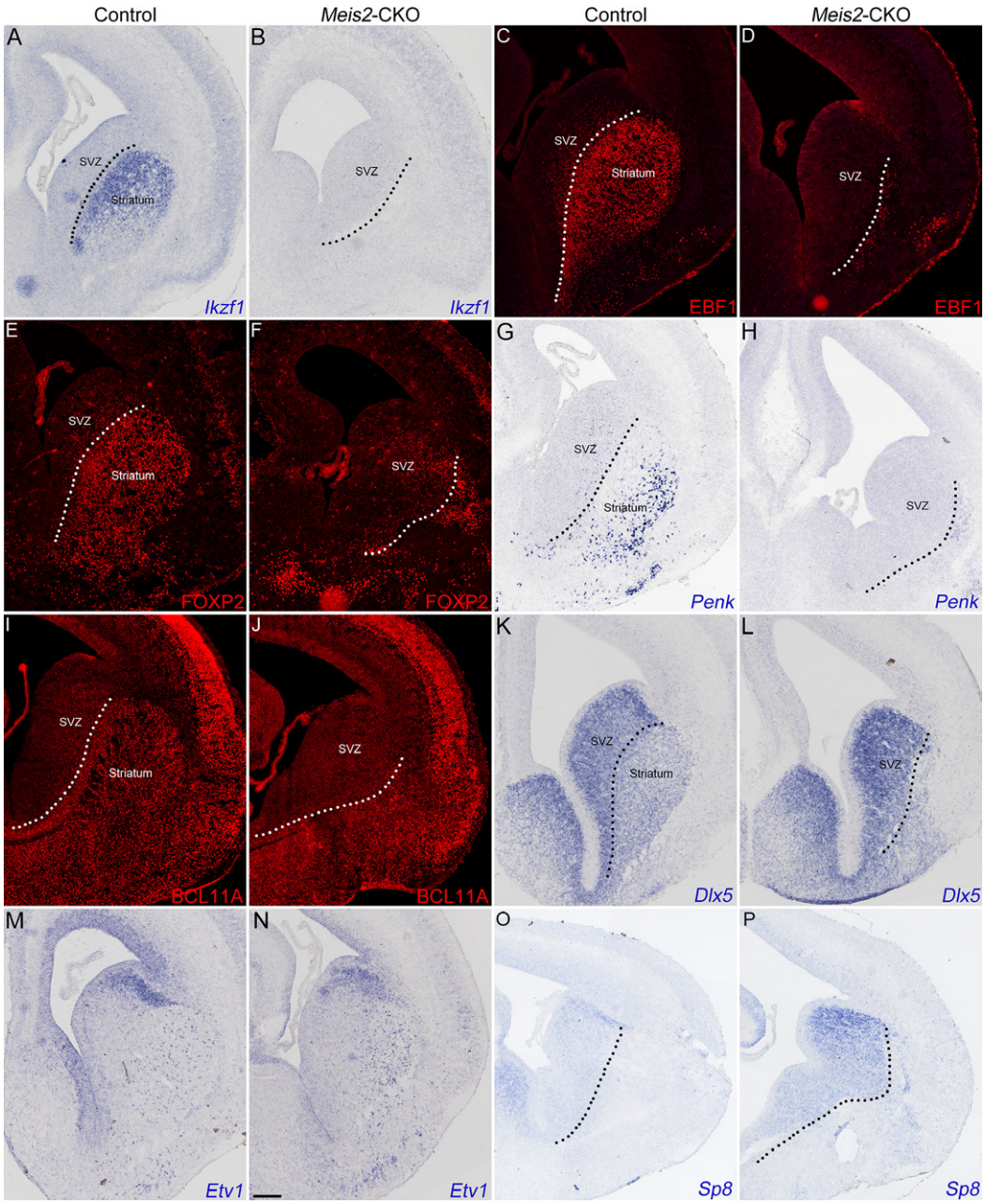

Fig. S2. *Meis2* is required for the generation of striatal MSNs

(A-J) At E16.5, the expression of *Ikzf1*, EBF1, FOXP2, *Penk* and BCL11A was greatly reduced in *Meis2*-CKO mice, compared to control mice. (K-L) Immature neurons that expressed *Dlx5* were generated in the LGE SVZ of *Meis2*-CKO mice. (M-N) There is no significant difference of the *Etv1* expression between *Meis2*-CKO mice and control mice. (O-P) The expression of the transcription factors *Sp8* are increased in the LGE. Scale bars: 200 μm in N for A-P.

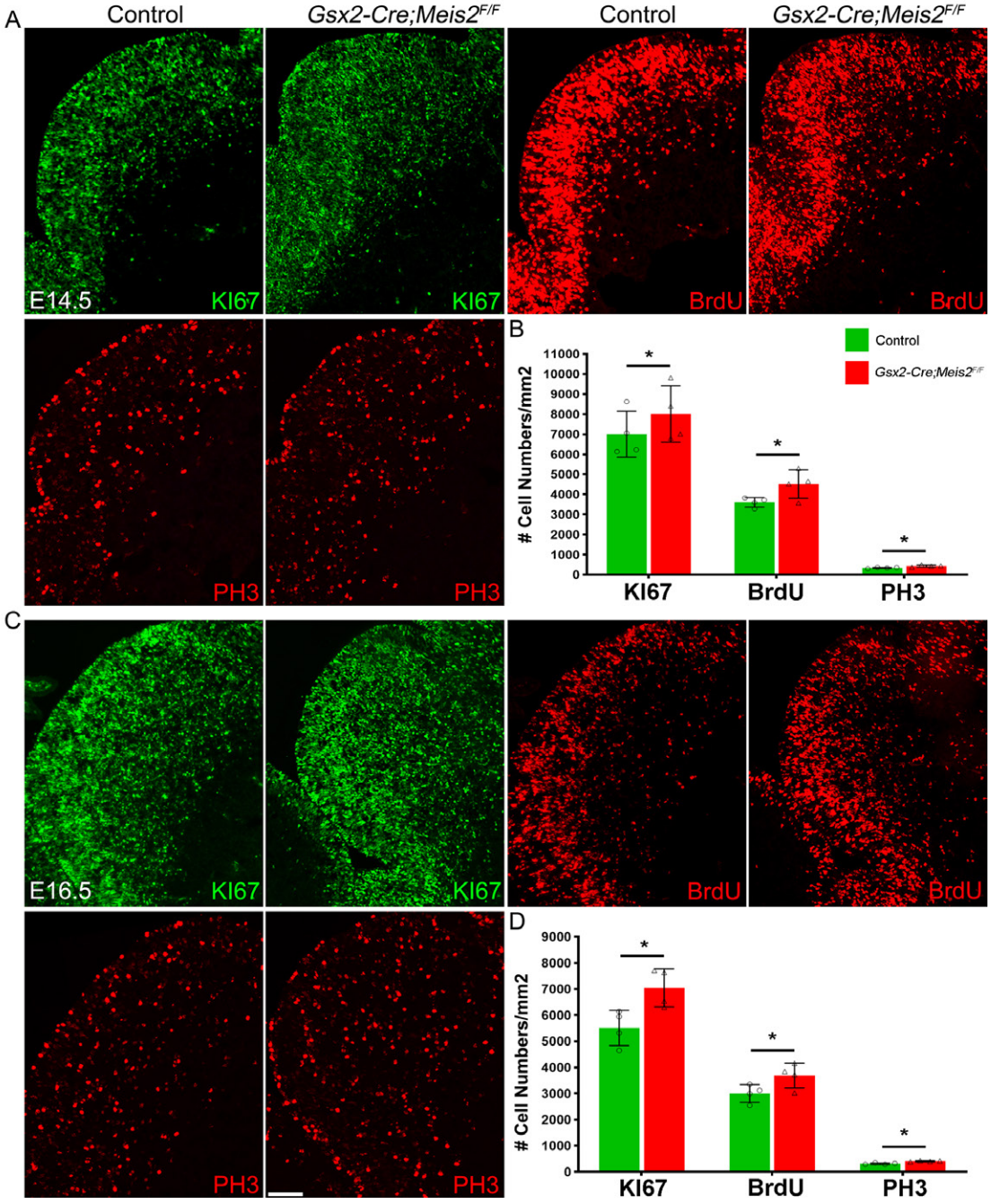

Fig. S3. Cell proliferation is also increased in *Gsx2-Cre; Meis2$^{F/F}$* mice

(A-B) At E14.5, the number of KI67^{+}, PH3^{+}, and BrdU^{+} (2 h) cells were increased in the LGE of *Gsx2-Cre; Meis2$^{F/F}$* mice versus control. (C-D) At E16.5, the numbers of KI67^{+}, PH3^{+}, and BrdU^{+} cells were also increased in the LGE of *Gsx2-Cre; Meis2$^{F/F}$* mice. Scale bars: 50 μm in C for A and C.

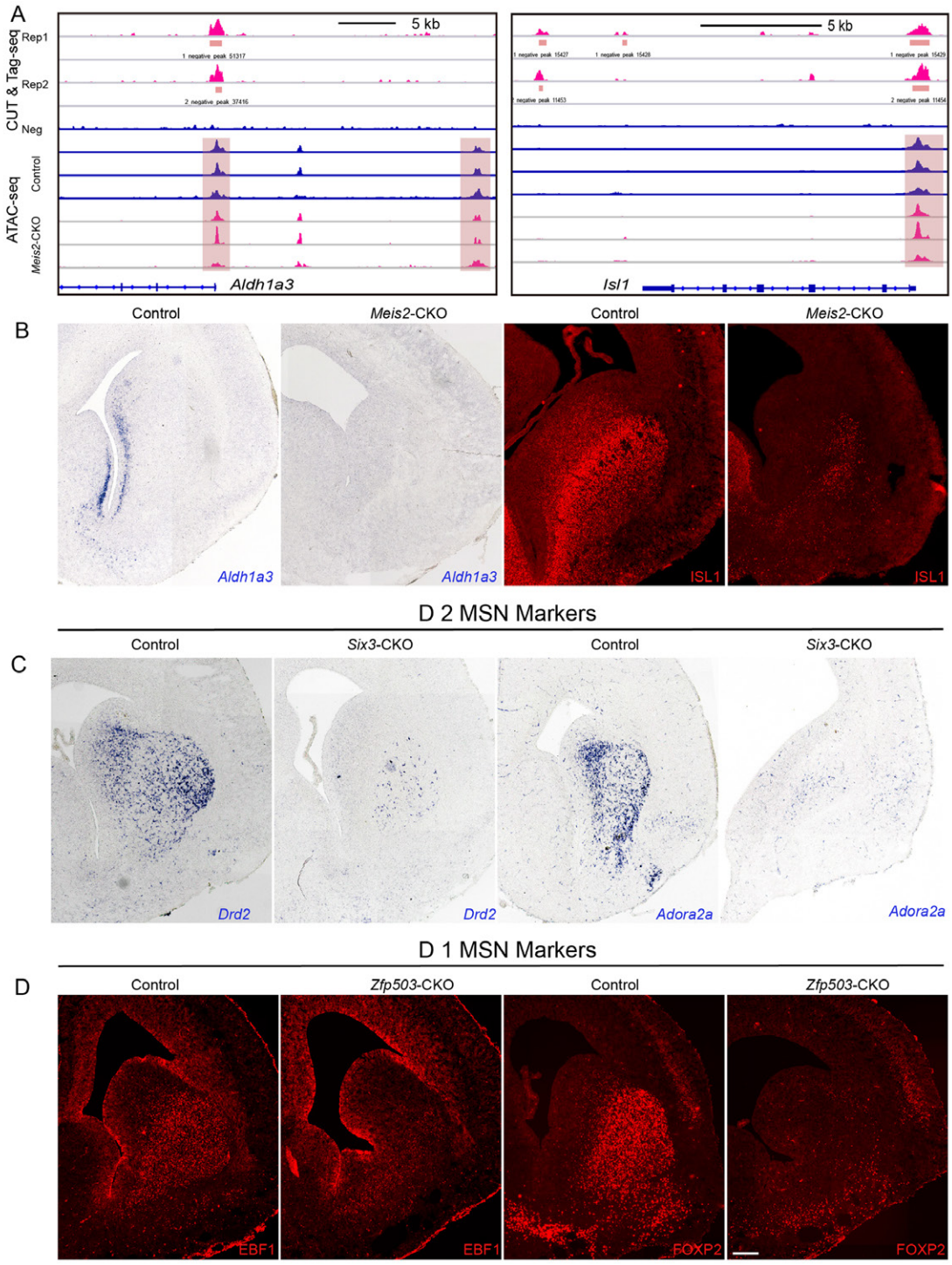

Fig. S4: *Meis2* is required for the normal differentiation process of the MSNs

(A) CUT&Tag-seq and ATAC-seq data showed that the expression of *Aldh1a3* and *Isl1* is directly regulated by *Meis2*. (B) At E16.5, the expression of *Aldh1a3* and *Isl1* was greatly reduced in *Meis2*-CKO mice compared to control mice. (C) ISH showed that the expression of *Drd2* and *Adora2a* was significantly reduced in the *Six3*-CKO mice. (D) Immunostaining showed that the expression of D1 MSN markers (EBF1 and FOXP2) was significantly reduced in *Zfp503*-CKO mice. N = 3 mice per group; Scale bar: 200 μm in D for B-D.

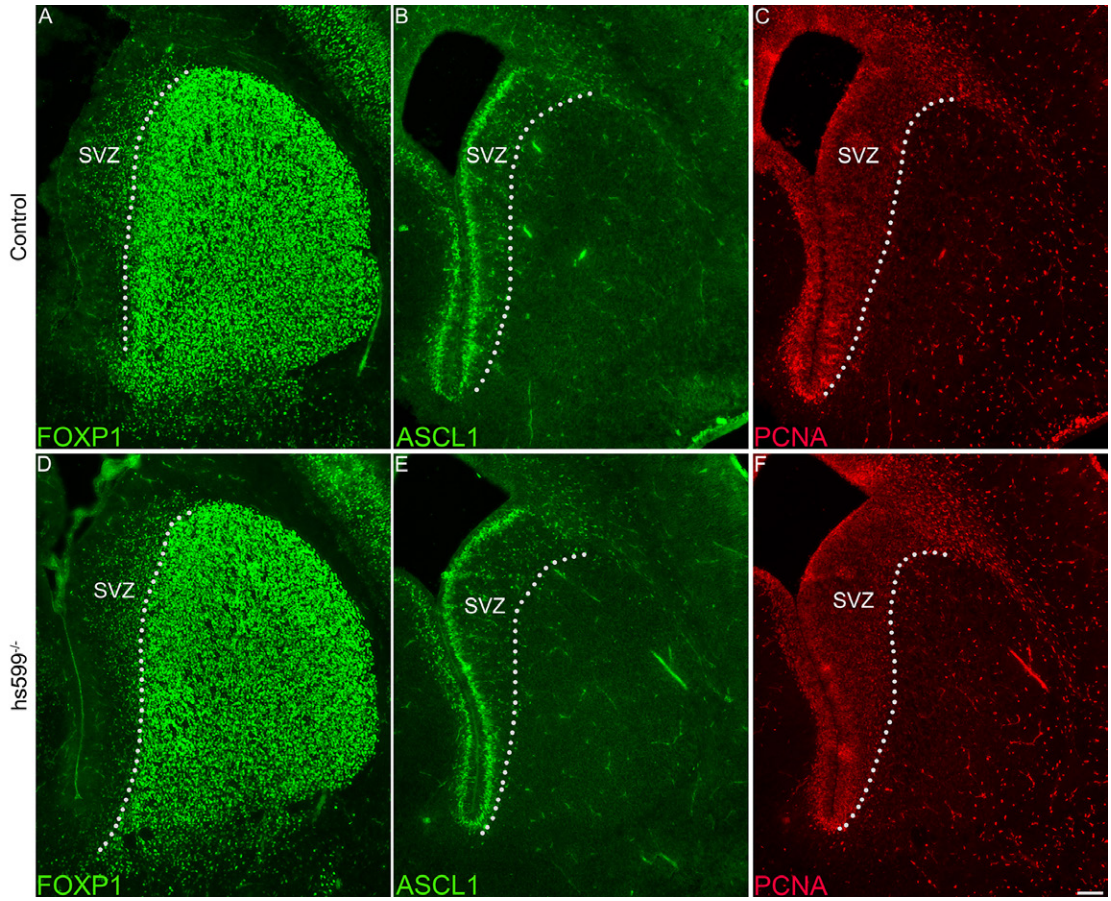

Fig. S5. The development of the striatal MSNs is not significantly changed in hs599$^{-/-}$ mice

(A, D) The expression of FOXP1 is not affected in the striatum of hs599 mutant mice at E16.5. (B-C, E-F) The expression of the ASCL1 and PCNA is slightly increased in the hs599 mutants compared to the control mice. Dotted lines mark the border of the LGE SVZ and striatum. Subventricular zone: SVZ. N = 3 mice per group; Scale bar: 100 μm in F for A-F.

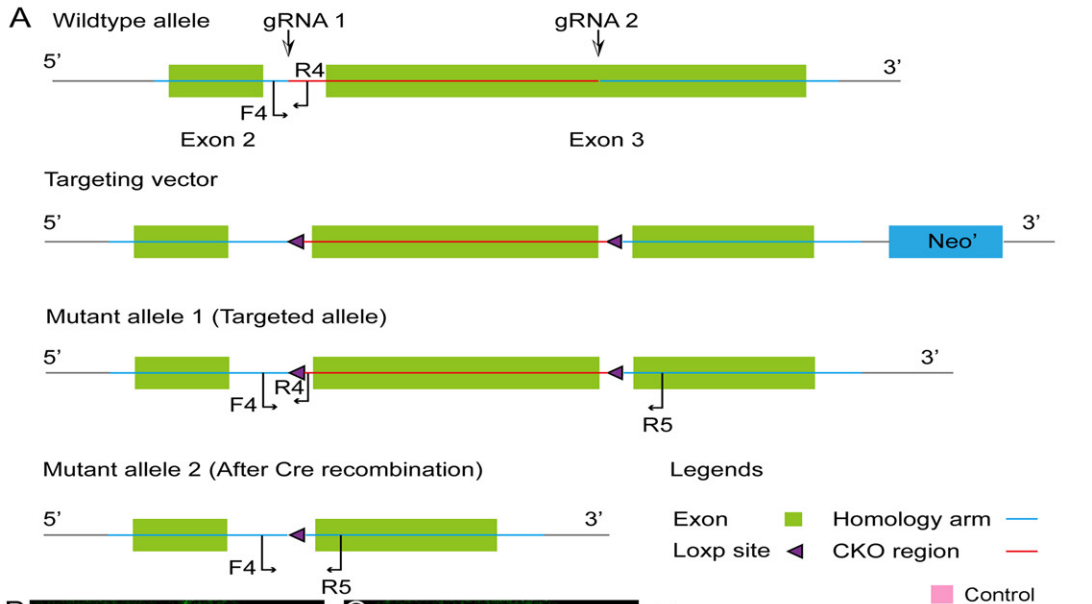

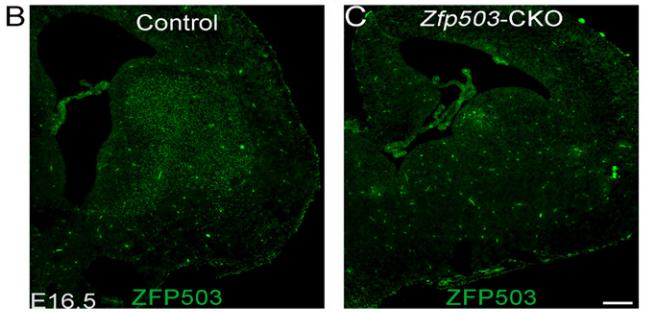

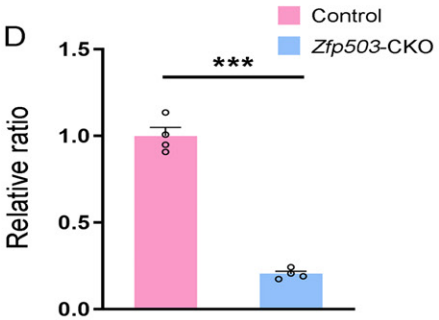

RNA design

E

Guide	Sequence (5'-3')
5'Guide #1	CACCGAGTAAGGTGACCAGC AGG
3'Guide #2	AAAAGAAGCGAAGGTCGGGA GGG

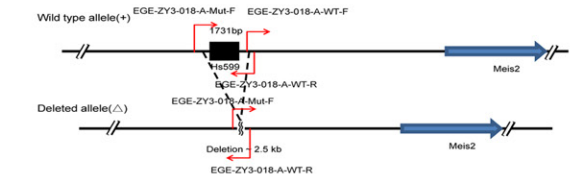

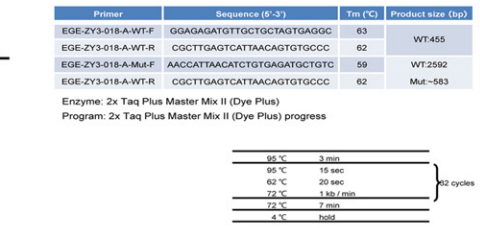

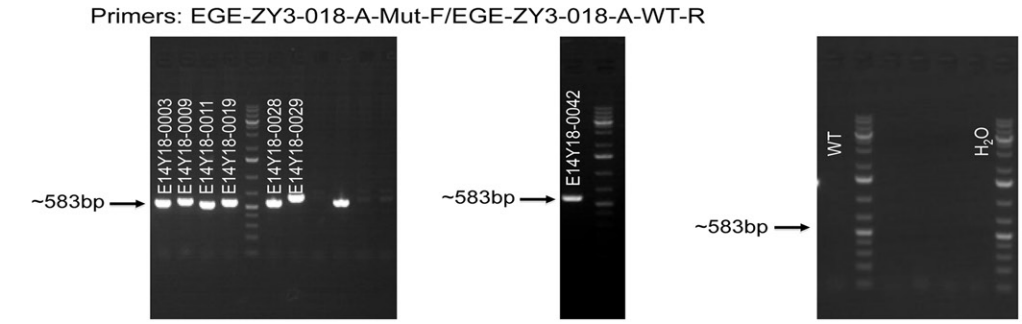

Fig. S6. Generation of *Zfp503*-CKO and *hs599*$^{+/-}$ mice

(A) Using the CRISPR/Cas9 strategy to generate *Zfp503*$^{F/+}$ mice. The coding region exon 3 was flanked by Loxp sites. After Cre recombination, exon 3 was deleted. (B-D) At E16.5, deletion of the *Zfp503* gene was confirmed at the protein level by immunostaining in the *Zfp503-CKO* striatum. ** $p < 0.01$, $n = 4$ per group; Scale bar, 200 µm. (E) The primer sequence of the gRNA. (F-H) Genotyping to confirm enhancer deletions and gel images showing genotyping results from wild-type (WT) and enhancer deletion mice. Genotyping from wild-type (WT) and enhancer deletion mice to confirm enhancer deletions and gel image.

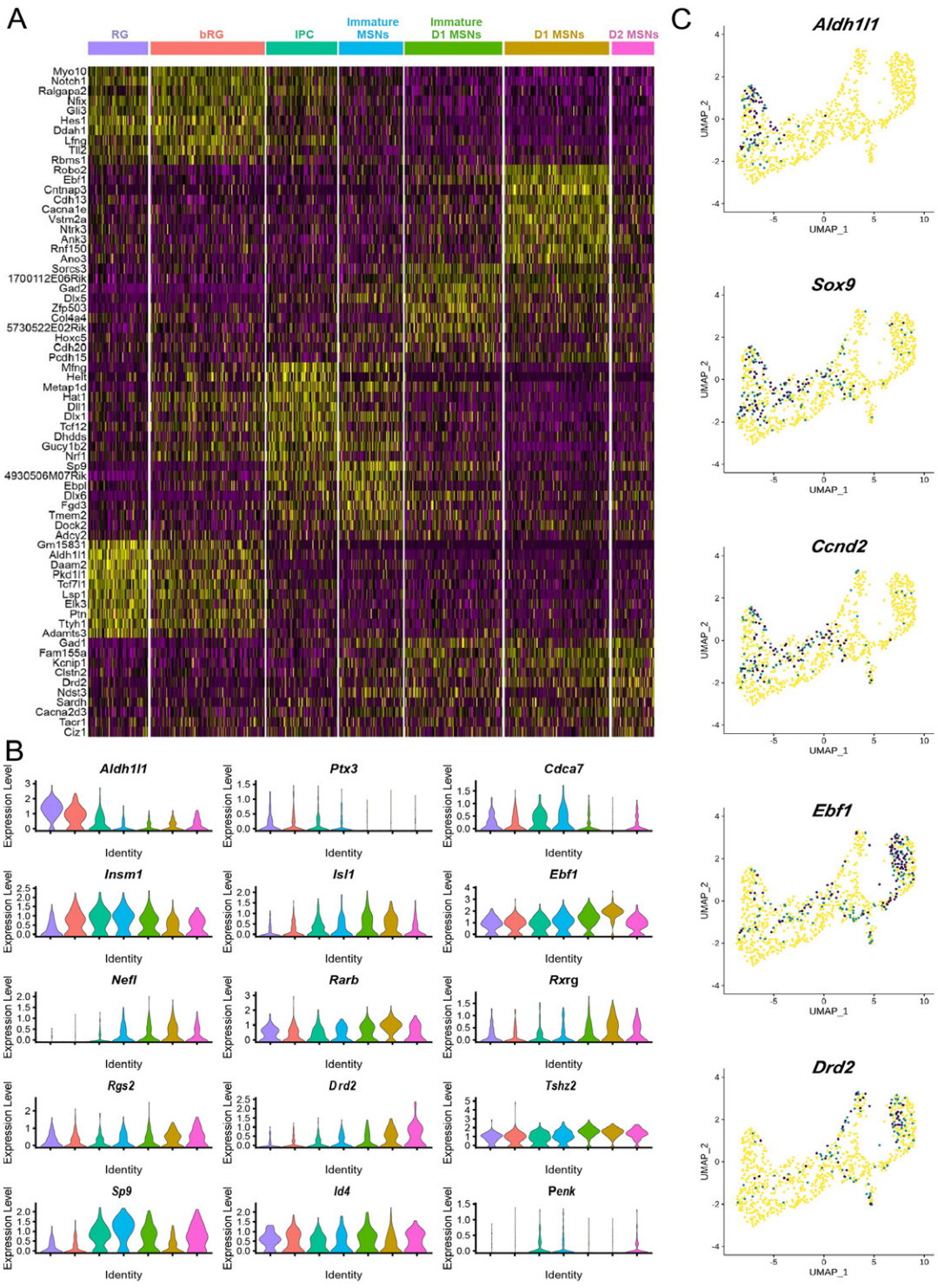

Fig. S7. Analysis of sc-ATAC-seq at E14.5

(A) Heat map showing the top 10 genes in the 7 clusters. (B) Violin plots showing the expression of the subtype cell markers. (C) UMAP plots showing distinct chromatin accessibility profiles of marker genes. progenitor cells.